

Second Generation Stars in Globular Clusters from Rapid Radiative Cooling of Pre-Supernova Massive Star Winds

Cassandra Lochhaas¹ and Todd A. Thompson¹

¹ *Department of Astronomy and the Center for Cosmology and Astroparticle Physics, The Ohio State University, 140 West 18th Avenue, Columbus, OH 43210, USA*

10 March 2022

ABSTRACT

Following work by Wünsch and collaborators, we investigate a self-enrichment scenario for second generation star formation in globular clusters wherein wind material from first generation massive stars rapidly radiatively cools. Radiative energy loss allows retention of fast winds within the central regions of clusters, where it fuels star formation. Secondary star formation occurs in $\sim 3 - 5$ Myr, before supernovae, producing uniform iron abundances in both populations. We derive the critical criteria for radiative cooling of massive star winds and the second generation mass as a function of cluster mass, radius, and metallicity. We derive a critical condition on M/R , above which second generation star formation can occur. We speculate that above this threshold the strong decrease in the cluster wind energy and momentum allows ambient gas to remain from the cluster formation process. We reproduce large observed second generation fractions of $\sim 30 - 80\%$ if wind material mixes with ambient gas. Importantly, the mass of ambient gas required is only of order the first generation’s stellar mass. Second generation helium enrichment ΔY is inversely proportional to mass fraction in the second generation; a large second generation can form with $\Delta Y \sim 0.001 - 0.02$, while a small second generation can reach $\Delta Y \sim 0.16$. Like other self-enrichment models for the second generation, we are not able to simultaneously account for both the full range of the Na-O anticorrelation and the second generation fraction.

Key words: galaxies: star clusters: general — galaxies: star formation — stars: winds, outflows

1 INTRODUCTION

Observations of globular clusters (GCs) imply that they contain more than a single simple stellar population. Star-to-star light element abundance variations, such as the O-Na and Mg-Al anticorrelations in red giants (Gratton et al. 2001; Carretta et al. 2009a), multiple main sequences (Bedin et al. 2004; Piotto et al. 2007), horizontal branches (Ferraro et al. 1998; D’Antona et al. 2002) and subgiant branches (Bedin et al. 2004; Villanova et al. 2007), and helium enrichment (D’Antona et al. 2005; Piotto et al. 2005) all indicate that each GC has at least two, and sometimes several, unique populations of stars. In most cases where just two stellar populations are identified, the so-called “second generation” stars are 0.5 – 3 times as prevalent as the “first generation” (Carretta et al. 2009a; Milone et al. 2017).

Proposed ideas for the evolution of GCs containing multiple stellar populations include accretion of interstellar matter after the first star formation episode (Bekki & Mackey

2009), cluster mergers (van den Bergh 1996), and several self-enrichment scenarios, in which ejecta from a first stellar generation fuels a second star formation episode. Light-element-enriched material is the result of hot H-burning mixed up to the convective zone of stars (Denisenkov & Denisenkova 1990). This material can then be expelled as winds from fast rotating stars (Decressin et al. 2007a,b), asymptotic giant branch (AGB) stars (Ventura et al. 2001; Conroy 2012), supermassive stars (Denissenkov & Hartwick 2014), massive binary stars (de Mink et al. 2009) or normal massive stars and supernovae (Maeder & Meynet 2006; Prantzos & Charbonnel 2006; Tenorio-Tagle et al. 2007; Wünsch et al. 2007, 2017).

All proposed scenarios have problems explaining some aspects of the observations (for recent reviews, see Bastian 2015; Gratton et al. 2012). In particular, there are four key issues facing all self-enrichment scenarios. First, the first-generation stars must supply enough material to form a

arXiv:1704.03469v2 [astro-ph.GA] 6 Jul 2017

massive second generation, which may include mixing with ambient gas. Second, the light element abundances of the second generation stars must match observations. These two points are closely tied, as the relative amounts of wind material and ambient gas affects both the abundances and size of the second generation. In order to produce second generation abundances matching observations from AGB or massive star wind material, GCs need to either have first stellar generations 10 – 100 times more massive at birth and have significantly decreased their total stellar mass by ejecting most of the first generation stars into the Milky Way halo (Martell et al. 2011; Schaerer & Charbonnel 2011; Carretta 2016), or have a very top-heavy initial mass function (IMF) (Conroy 2012; Decressin et al. 2007b). The third key issue is that wind speeds near or exceeding the escape velocity of GCs — e.g., 10–30 km s⁻¹ for AGB winds (Loup et al. 1993) or 1000 – 2000 km s⁻¹ for massive star winds (Lamers et al. 1995) — make it difficult for the shallow gravitational potential wells of GCs to retain wind material. Fourth, the second generation must form without supernova ejecta, since the stars in GCs have uniform iron abundances (see review by Suntzeff 1993 and references therein, Carretta et al. 2009b; exceptions are ω Cen, Gratton 1982 and Johnson & Pila-chowski 2010, and others, Johnson et al. 2015).

We investigate a scenario for second generation formation explored by Wünsch et al. (2008); Palouš et al. (2014); Wünsch et al. (2017) in which massive star winds from the first stellar generation shock and thermalize to produce a region of hot gas in the cluster interior on Myr timescales after the first generation’s formation. If the mass loss rate is high enough or if the winds mix with ambient gas left over from cluster formation, the gas is dense enough to become radiative, loses its thermal energy, and can be retained in the GC to fuel a subsequent generation of star formation. The action of rapid radiative cooling eliminates the wind retention problem. We show that in order for radiative cooling to set in and form a second stellar generation 0.5 – 3 times as massive as the first, wind mass-loading factors must be $\sim 20 - 100$. This is achievable if the wind ejecta mixes with an ambient gas mass of order the first generation stellar mass, less if wind mass loss rates are higher than current stellar evolution models suggest. The ambient gas may be left over from the first stellar formation episode. In our picture, the GC does not need to have a larger first generation at birth than observed in GCs today, does not need a top-heavy IMF, and does not need to eject first generation stars. Finally, second generation formation occurs only within the first few Myr after the GC’s birth, before supernovae from the most massive stars occur, so that there is no additional Fe enrichment in the second generation. Clusters likely blow out the remnants of their natal gas cloud ~ 5 Myr after formation (Bastian et al. 2014), halting any additional second generation formation.

In section 2, we estimate a critical condition for cooling of gas deposited by massive star winds forming a second stellar generation. We make predictions for the required mass-loading factor and size of the second generation as functions of the GC’s mass and radius, derive a critical condition on the cluster’s stellar mass per unit radius M/R for cooling to set in, compare to observations of M/R and second-generation stellar fraction in GCs, and compare the observed helium and other light element abundance spreads

to abundances in our model. In section 3, we discuss outstanding problems, uncertainties, and how changes to our assumptions impact our model. Section 4 gives our conclusions.

2 THE MODEL

2.1 Critical Condition for Cooling

We wish to estimate the size of the region within the cluster that radiatively cools as a function of cluster properties. For low enough densities, the material should never be radiative and the thermalized winds will drive a fast cluster wind (Silich et al. 2003, 2004). For higher densities, radiative cooling should first set in at the cluster center, while the outer lower density regions continue to drive an outflow (Tenorio-Tagle et al. 2005, 2007; Wünsch et al. 2007, 2008). Finally, for higher density, a substantial fraction of the cluster’s gas will cool and self-shield (Palouš et al. 2014; Wünsch et al. 2017), leading to star formation. We assume spherical symmetry, uniform mass and energy deposition, and no gravity. If the massive star wind ejecta with total kinetic power \dot{E}_{tot} thermalizes, the asymptotic cluster wind velocity from energy conservation is

$$\frac{1}{2}\dot{M}_{\text{tot}}v_{\infty}^2 = \dot{E}_{\text{tot}} \quad \implies \quad v_{\infty} = \left(2\frac{\alpha}{\beta}\frac{\dot{E}_w}{\dot{M}_w}\right)^{\frac{1}{2}} \quad (1)$$

where \dot{M}_w is the mass deposition rate from massive star winds, \dot{M}_{tot} is the *total* mass deposition rate, which may include wind material and swept-up ambient cluster gas, and the mass-loading factor β is the ratio between the two, such that $\dot{M}_{\text{tot}} = \beta\dot{M}_w$. β represents any additional mass deposition other than the \dot{M}_w defined in equation (3), which may be ambient gas or additional stellar wind mass loss. \dot{E}_w is the wind energy deposition, α is the efficiency of thermalization such that the total energy deposition is $\dot{E}_{\text{tot}} = \alpha\dot{E}_w$. In the absence of radiative cooling, the hot, thermalized gas inside the cluster will expand out from the edge of the cluster, driving a supersonic wind. The sonic point will be located at the edge of the energy and mass deposition region at R_{cl} (Chevalier & Clegg 1985; Wang 1995; Silich et al. 2004). Using the fact that the Bernoulli integral is constant for $r > R_{cl}$ and that the sonic point is at R_{cl} , $c_s^2 = v_{\infty}^2/4$ at $r = R_{cl}$ for $\gamma = 5/3$, where v_{∞}^2 is given in equation (1). This allows us to write the temperature and pressure in terms of α , β , \dot{E}_w , and \dot{M}_w . Given mass conservation, we can also find the density at R_{cl} .

The conditions for radiative cooling vary within the cluster because the density and temperature vary with position, and depend on the radial distribution of \dot{E}_{tot} and \dot{M}_{tot} per volume. For constant volumetric energy and mass injection rates, Chevalier & Clegg (1985) derived the self-similar solution for pressure, density, and wind velocity. We use values from Chevalier & Clegg (1985) to scale the density and temperature at R_{cl} to values within the cluster: $T(r < R_{cl}) \approx \zeta_T T(R_{cl})$ and $\rho(r < R_{cl}) \approx \zeta_{\rho} \rho(R_{cl})$. Values of $\zeta_{\rho} = 2.07$ and $\zeta_T = 1.28$ are the averages of the scalings found in Chevalier & Clegg (1985) between 10% and 80% of the cluster’s volume (corresponding to radii within the cluster of $0.46R_{cl}$ and $0.93R_{cl}$). We use these as representative values throughout. For a different model of the

radial dependence of the mass and energy injection rate per unit volume, ζ_ρ and ζ_T will change and may be functions of the radius within the cluster (see Appendix of Zhang et al. 2014). Hydrodynamical calculations should assess the role of multidimensional effects like clumping (e.g., Wünsch et al. 2017).

As a reference point, we adopt values for \dot{E}_w and \dot{M}_w as the average values from 2.5 Myr to 7 Myr given by a combination of the codes STARBURST99 (Leitherer et al. 1999, 2014) and BPASS (Eldridge et al. 2008; Eldridge & Stanway 2009) for an instantaneously-formed $10^5 M_\odot$ GC with a double power law initial mass function (IMF), with power law index for dN/dM of -1.3 between $0.1M_\odot$ and $0.5M_\odot$ and -2.35 between $0.5M_\odot$ and $120M_\odot$, at one-tenth solar metallicity. Although the relation between initial mass and the probability of black hole formation is complicated (Pejcha & Thompson 2015; Sukhbold et al. 2016), we set the mass cutoff for direct collapse to black hole at $25M_\odot$, which means the first supernova can be expected at ~ 7 Myr. Before 2.5 Myr, the mass deposition rates are low enough to be negligible because stars have not yet entered post-main sequence evolution. We mix the two codes by assuming a 50% binary fraction, and we have selected only those binaries in BPASS with mass ratio 0.9 and period 10^4 days. Other mass ratios and periods vary the STARBURST99 and BPASS combined average mass loss rates from $10^{-3.4} M_\odot \text{ yr}^{-1}$ to $10^{-3.1} M_\odot \text{ yr}^{-1}$, so we pick the period and mass ratio combination that maximizes \dot{M}_w . Shorter binary periods decrease the average \dot{M}_w slightly. The BPASS code examines binary mass loss as a function of system mass, which is useful for constructing a GC with a specific IMF. However, de Mink et al. (2009) proposes that massive binaries in a cluster produce a total wind mass that contains 13% of the first generation stellar mass, implying a mass loss rate of $\sim 10^{-2.5} M_\odot \text{ yr}^{-1}$, 0.6 dex higher than our fiducial mass loss rate, so the rates we use here may be somewhat conservative. The amount of wind ejecta relative to the amount of ambient gas swept up is crucial in determining the helium enrichment of the second generation. For this reason, we consider enhancements to our fiducial \dot{M}_w in §2.4, and we consider the maximum possible mass loss rate for a massive star population.

Only STARBURST99 provides energy deposition rates, and so we assume this \dot{E}_w for the binary stars from BPASS. We further assume both \dot{E}_w and \dot{M}_w scale linearly with cluster mass above $10^4 M_\odot$, as long as the IMF is fully populated.

The average values¹ for our fiducial cluster are then

$$\dot{E}_w = 10^{37.8} \text{ ergs s}^{-1} \left(\frac{M_1}{10^5 M_\odot} \right) \quad (2)$$

$$\dot{M}_w = 10^{-3.1} M_\odot \text{ yr}^{-1} \left(\frac{M_1}{10^5 M_\odot} \right) \quad (3)$$

where M_1 is the mass of the first generation of stars, which is the total stellar mass of the cluster before formation of the second stellar generation. For these values, $v_\infty \approx 500 \text{ km s}^{-1}$ (eq. 1). We also explore an additional value for the cluster metallicity closer to solar for comparison. For metallicity $0.7Z_\odot$, $\dot{E}_w = 10^{38.7} \text{ ergs s}^{-1}$ ($M_1/10^5 M_\odot$) and $\dot{M}_w = 10^{-3.0} M_\odot \text{ yr}^{-1}$ ($M_1/10^5 M_\odot$), implying $v_\infty \approx 1200 \text{ km s}^{-1}$. Our fiducial cluster has a first generation stellar mass $M_1 = 10^5 M_\odot$, half-light radius $R_{cl} = 1 \text{ pc}$, one-tenth solar metallicity, and efficiency of energy thermalization $\alpha = 0.1$, but we explore different values throughout.

Because the advection time is larger than the heating time throughout most of the cluster volume (Chevalier & Clegg 1985), we neglect the kinetic energy of the thermalized gas and assume the cluster cools radiatively if the volumetric cooling rate is larger than the volumetric heating rate \dot{E}_{tot} : $\Gamma_{\text{cool}} \geq \Gamma_{\text{heat}}$. For the purposes of an analytic estimate, we approximate the cooling rate as a double power-law below 10^7 K (Draine 2011),

$$\Gamma_{\text{cool}} = \begin{cases} \Lambda_0 \left(\frac{T_0}{T} \right)^{0.7} n^2 & 10^5 < T < 10^7 \text{ K} \\ \Lambda'_0 \left(\frac{T}{T'_0} \right)^p n^2 & 10^4 < T < 10^5 \text{ K} \end{cases} \quad (4)$$

where n and T are the number density and temperature of the gas. At one-tenth solar metallicity, $\Lambda_0 \simeq 2.2 \times 10^{-23} \text{ ergs s}^{-1} \text{ cm}^3$, $T_0 = 10^6 \text{ K}$, $\Lambda'_0 \simeq 1.1 \times 10^{-22} \text{ ergs s}^{-1} \text{ cm}^3$, $p = 0.3$, and $T'_0 = 10^5 \text{ K}$; at 0.7 solar metallicity, $\Lambda_0 \simeq 9.0 \times 10^{-23} \text{ ergs s}^{-1} \text{ cm}^3$, $T_0 = 10^6 \text{ K}$, $\Lambda'_0 \simeq 4.5 \times 10^{-22} \text{ ergs s}^{-1} \text{ cm}^3$, $p = 0.9$, and $T'_0 = 10^5 \text{ K}$. The local heating rate is

$$\Gamma_{\text{heat}} = \frac{3\alpha \dot{E}_w}{4\pi R_{cl}^3}. \quad (5)$$

We will focus on one-tenth solar metallicity and $T > 10^5 \text{ K}$, but the following derivation is similar, with only differing exponential powers, for different metallicities and temperatures. Setting the heating and cooling rates equal allows us to derive the critical condition for cooling:

$$\frac{3\alpha \dot{E}_w}{4\pi R_{cl}^3} = \Lambda_0 \left(\frac{T_0}{T} \right)^{0.7} n^2 \quad (6)$$

The density inside the thermalized region is $n \simeq \zeta_\rho n(R_{cl})$,

¹ We find the average values of \dot{E}_w and \dot{M}_w by summing the total energy and mass deposition from both STARBURST99 and BPASS, then dividing by the total time from cluster formation to first supernova. BPASS examines single binary systems with discrete masses, not a full binary stellar population. We combine the BPASS systems into a full cluster by integrating with our IMF, but the system masses examined in BPASS sparsely sample the IMF at the high mass end. This produces a bursty total mass- and energy-loss rate over the full evolution of the cluster, but with a well-defined average value given in equations (2) and (3). Including the BPASS code in our calculation increases \dot{M}_w by 0.4 dex over just STARBURST99 for $Z = 0.1Z_\odot$, and by 0.1 dex for $Z = 0.7Z_\odot$.

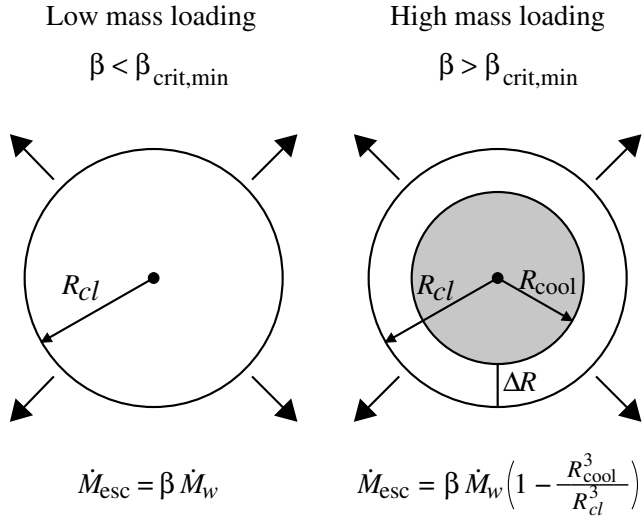


Figure 1. A cartoon showing the two scenarios of massive star winds depositing energy and mass in a region of size R_{cl} . On the left, there is not enough mass loading of the winds ($\beta < \beta_{crit,min}$) and all deposited mass exits the cluster as a wind. On the right, $\beta > \beta_{crit,min}$ and the inner shaded region within R_{cool} (see equation 10) cools and is retained in the cluster while any mass deposited in the outer region between R_{cool} and R_{cl} escapes the cluster as a wind. The critical β for a given ΔR is given in equation (12).

where

$$n(R_{cl}) = \frac{\beta \dot{M}_{esc}}{4\pi R_{cl}^2 \mu m_p c_s}, \quad (7)$$

where \dot{M}_{esc} is the mass deposition rate of only that material that escapes the cluster as a wind (the gas that does not cool radiatively). The temperature of thermalized gas is given by

$$T = \zeta_T \frac{3}{5} \frac{\mu m_p}{k_B} c_s(R_{cl})^2 = \zeta_T \frac{3}{10} \frac{\mu m_p}{k_B} \frac{\alpha \dot{E}_w}{\beta \dot{M}_w}. \quad (8)$$

Scaling this to our fiducial cluster yields

$$T \sim 4 \times 10^5 \text{ K} \frac{\alpha_{0.1}}{\beta_2}, \quad (9)$$

where $\alpha_{0.1} = \alpha/0.1$ and we have anticipated the mass loading factor needed for most of the cluster volume to cool (see eq. 12) and scaled to $\beta_2 = \beta/2$.

We define a cooling radius R_{cool} such that all mass and energy deposited within this radius cools and stays within the cluster, whereas all mass and energy deposited outside R_{cool} escapes as a wind. Since we assume uniform mass and energy deposition everywhere within R_{cl} , $\dot{M}_{esc} = \beta \dot{M}_{tot} \left[1 - \left(\frac{R_{cool}}{R_{cl}} \right)^3 \right]$ (see Figure 1).

Substituting equations (7) and (8) into equation (6) and solving for R_{cool} yields

$$\left(\frac{R_{cool}}{R_{cl}} \right)^3 = 1 - \sqrt[3]{\left(\frac{3\zeta_T}{10k_B T_0} \right)^{0.7} \frac{6\pi(\mu m_p)^{2.7} R_{cl} \alpha^{2.7} \dot{E}_w^{2.7}}{\Lambda_0 \beta^{3.7} \dot{M}_w^{3.7} \zeta_\rho^2}}. \quad (10)$$

Solving for the critical β value needed for a given R_{cool} yields

$$\beta_{crit}^{3.7} = \left(\frac{3\zeta_T}{10k_B T_0} \right)^{0.7} \frac{6\pi(\mu m_p)^{2.7} R_{cl} \alpha^{2.7} \dot{E}_w^{2.7}}{\Lambda_0 \dot{M}_w^{3.7} \left[1 - \left(\frac{R_{cool}}{R_{cl}} \right)^3 \right]^2 \zeta_\rho^2}. \quad (11)$$

In the limit that the cooling radius approaches R_{cl} , $\left[1 - \left(\frac{R_{cool}}{R_{cl}} \right)^3 \right]^2 \approx 9 \left(\frac{\Delta R}{R_{cl}} \right)^2$, where $\Delta R = R_{cl} - R_{cool}$. Scaling this limit to our fiducial globular cluster properties, we find

$$\beta_{crit} \sim 2 \alpha_{0.1}^{0.73} \left(\frac{R_{cl}}{\text{pc}} \right)^{0.81} \left(\frac{10^5 M_\odot}{M_1} \right)^{0.27} \left(\frac{0.1 \text{ pc}}{\Delta R} \right)^{0.54} \quad (12)$$

for one-tenth solar metallicity gas and $\mu = 1.38$. If $\beta \geq \beta_{crit}$, the gas within R_{cool} radiatively cools and fuels the second generation of star formation. In the limit $R_{cool} \rightarrow 0$, we find²

$$\beta_{crit,min} \sim 1 \alpha_{0.1}^{0.73} \left(\frac{R_{cl}}{\text{pc}} \right)^{0.27} \left(\frac{10^5 M_\odot}{M_1} \right)^{0.27}. \quad (13)$$

If $\beta < \beta_{crit,min}$, none of the gas in the cluster cools, and no second generation of star formation occurs. Note that the critical value for β for nearly all of the cluster volume to cool is just $\sim 2 \times \beta_{crit,min}$. We can rearrange equation (13) to find a condition on M_1 and R_{cl} for cooling for a given α and β :

$$\left[\frac{M_1}{R_{cl}} \right]_{crit,min} \sim 10^5 M_\odot \text{ pc}^{-1} \alpha_{0.1}^{2.7} \beta^{-3.7}. \quad (14)$$

If the combination of first-generation mass and cluster radius are not larger than $\left[\frac{M_1}{R_{cl}} \right]_{crit,min}$ for a given α and β , then we would not expect a second generation of stars to form at all in that cluster. Similarly, we can rewrite equation (12) to find a condition on M_1 and R_{cl} for nearly all of the cluster to cool for a given α and β :

$$\left[\frac{M_1}{R_{cl}} \right]_{crit} \sim 2.3 \times 10^5 M_\odot \text{ pc}^{-1} \frac{\alpha_{0.1}^{0.9}}{\beta^{1.2}} \times \left(\frac{M_1}{10^5 M_\odot} \right)^{0.67} \left(\frac{0.1 \text{ pc}}{\Delta R} \right)^{0.67}. \quad (15)$$

Equations (12) and (13) imply that for a significant fraction of the cluster's gas to cool, \dot{M}_w must be of order the fiducial value from standard population synthesis models. More massive and more compact clusters have a lower critical mass-loading (smaller β_{crit} and $\beta_{crit,min}$) for cooling, due to a greater number of massive stars depositing more wind material in a smaller volume. As an aside, note that β_{crit} in equation (12) diverges as $\Delta R \rightarrow 0$ because winds from stars at the edge of the cluster always drive a cluster outflow, but with smaller and smaller \dot{M}_{esc} as $R_{cool} \rightarrow R_{cl}$. Formally, no amount of mass-loading can make $R_{cool} = R_{cl}$ in the limit of an infinite number of sources, provided constant \dot{E}_w and \dot{M}_w throughout R_{cl} . However, even $\beta \sim 2 \times \beta_{crit,min}$ yields a cluster where a large fraction of the volume cools. Note also that R_{cl} does not necessarily have to be the edge of the

² We rearranged our equation for $\beta_{crit,min}$ to instead solve for \dot{E}_{crit} and compared with L_{crit} from [Wünsch et al. \(2007\)](#). For similar GC properties, we find our calculation and its scaling with GC parameters agree.

GC; it is the edge of the region where massive star winds are depositing mass and energy. If there is mass segregation for the massive stars, as seen in e.g. 47 Tuc (Zhang et al. 2015), R_{cl} could be smaller than the size of the GC we see today, which would decrease β_{crit} and $\beta_{crit,min}$.

The deposited wind mass that does not cool and escapes the cluster as a wind is $\dot{M}_{esc} = \beta \dot{M}_w (1 - R_{cool}^3/R_{cl}^3)$. For $\beta \lesssim \beta_{crit,min}$, $\dot{M}_{esc} \sim \beta \dot{M}_w$. As β increases, $R_{cool} \rightarrow R_{cl}$, and $\dot{M}_{esc} \ll \beta \dot{M}_w$. The cluster wind kinetic luminosity,

$$\begin{aligned} \dot{E}_{esc} &= \frac{1}{2} \dot{M}_{esc} v_\infty^2 \\ &\approx 10^{36} \text{ ergs s}^{-1} \frac{\alpha_{0.1}^{2.35}}{\beta_2^{1.85}} \\ &\times \left(\frac{\dot{E}_w}{10^{37.8} \text{ ergs s}^{-1}} \right)^{2.35} \left(\frac{\dot{M}_w}{10^{-3.1} M_\odot \text{ yr}^{-1}} \right)^{-1.85} \left(\frac{R_{cl}}{1 \text{ pc}} \right)^{0.5}, \end{aligned} \quad (16)$$

and momentum ejection rate,

$$\begin{aligned} \dot{p}_{esc} &= \dot{M}_{esc} v_\infty \\ &\approx 3 \times 10^{29} \text{ dynes s}^{-1} \frac{\alpha_{0.1}^{1.85}}{\beta_2^{1.35}} \\ &\times \left(\frac{\dot{E}_w}{10^{37.8} \text{ ergs s}^{-1}} \right)^{1.85} \left(\frac{\dot{M}_w}{10^{-3.1} M_\odot \text{ yr}^{-1}} \right)^{-1.35} \left(\frac{R_{cl}}{1 \text{ pc}} \right)^{0.5}, \end{aligned} \quad (17)$$

are thus dramatically reduced for $\beta \gtrsim \beta_{crit,min}$, since \dot{M}_{esc} rapidly decreases as $R_{cool} \rightarrow R_{cl}$. We thus hypothesize that for $\beta \gtrsim \beta_{crit,min}$, the cluster is much more likely to retain ambient gas from the cluster formation process. Therefore, although highly dependent on α and β , equation (14) gives the critical value of M_1/R_{cl} above which second generation star formation may occur.

Figure 2 shows the ratio of the cooling rate to the heating rate as a function of β for our fiducial GC for two energy thermalization efficiencies and two metallicities. The cooling rates were calculated at $0.93R_{cl}$, which contains 80% of the cluster's volume. $\Gamma_{cool}/\Gamma_{heat} = 1$ at $\beta = \beta_{crit}$. A cluster with a low energy thermalization efficiency and a low metallicity requires a lower β to obtain radiative cooling of 80% of its volume than a cluster with high α and high Z .

β_{crit} and $\beta_{crit,min}$ both depend on the normalization of the cooling function to the power of ≈ -0.27 , so naively a higher metallicity will reduce the critical mass-loading value. However, clusters with higher metallicity also have higher \dot{M}_w by a factor of 1.4 and higher \dot{E}_w by a factor of 7.4 in STARBURST99 (see discussion after equations 2 and 3), and the combined effect seen in Figure 2 shows that lower metallicity clusters will have lower β_{crit} . Most GCs have metallicities down to $[\text{Fe}/\text{H}] \sim -2$, whereas our fiducial GC has a metallicity of $[\text{Fe}/\text{H}] \sim -1$, so values of $\beta_{crit,min}$ and β_{crit} may be lower than what we report in equations (12) and (13) for GCs with similar masses and radii.

Figure 3 summarizes how the critical mass-loading depends on various properties of the cluster. Our fiducial cluster has $\beta_{crit} \sim 2$, so the temperature of the wind material and ambient gas mixture for $\beta = \beta_{crit}$ is $T \approx 4 \times 10^5$ K, putting it firmly within the region of the cooling function dominated by metal-line cooling. Since more massive clusters have lower β_{crit} , the temperature of wind material in these clusters is higher. A very massive and compact cluster

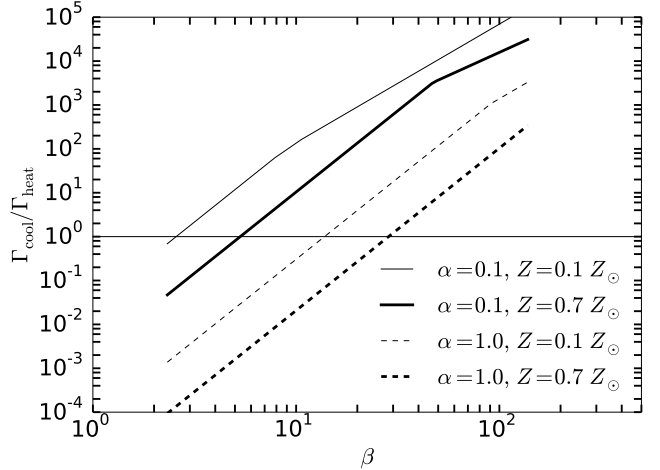


Figure 2. The ratio of cooling rate (Γ_{cool}) to heating rate (Γ_{heat}) of massive star winds within 80% of the cluster's volume ($R_{cool} = 0.93R_{cl}$) as a function of β , for energy thermalization efficiencies $\alpha = 0.1$ (solid) and $\alpha = 1.0$ (dashed) and metallicities one-tenth solar (thin lines) and 0.7 solar (thick lines). This is our fiducial cluster with mass and radius $10^5 M_\odot$ and $R_{cl} = 1$ pc.

with $M_1 = 10^7 M_\odot$ and $R_{cl} = 0.1$ pc has $\beta_{crit} \approx 0.3$ and thus $T \approx 3 \times 10^6$ K, which is close to the minimum of the cooling function at $\sim 10^7$ K, where this power-law approximation breaks down, and above which bremsstrahlung dominates. Thus, our model is more accurate for massive GCs, where a higher β is necessary for cooling.

2.2 Mass of the Second Generation

As shown in equations (12) and (13), for $\beta = \beta_{crit}$ or $\beta_{crit,min}$, the mass deposition rate of massive stars must be approximately that of current models. However, a much larger β is required for the second stellar generation to be as large as observed in globular clusters. If $\beta \approx \beta_{crit}$ ($R_{cool} \approx 0.93R_{cl}$) during the few Myr of post-main sequence massive star evolution, the total mass that cools to form a second generation would be $M_2 \approx 10^{3.7} M_\odot$, implying a second generation mass fraction of $M_2/M_1 \sim 0.05$, too small to explain the large second generation masses observed. In §2.4, we estimate a maximum upper bound on the wind mass loss rate and find that it can only be ~ 3 times higher than equation (3), implying that winds alone can only produce a second generation $\sim 0.05 \times 3 \sim 0.15$ as massive as the first generation³.

To produce the large mass loadings required by the observations requires mixing with a substantial reservoir of ambient gas, presumably left over from first generation formation. We wish to give ourselves the flexibility to consider both enhanced mass loss rates during the post-main-sequence evolution of massive stars *and* mixing with an amount of ambient gas in order to explore the relative impor-

³ Our calculation agrees with the numerical results of Wünsch et al. (2017) (see their Figure 10) for $\alpha = 0.1$ (their $\eta_{he} = 0.1$ and $\beta = 1$ or 3 (their $\eta_{ml} = 0$ or 2)).

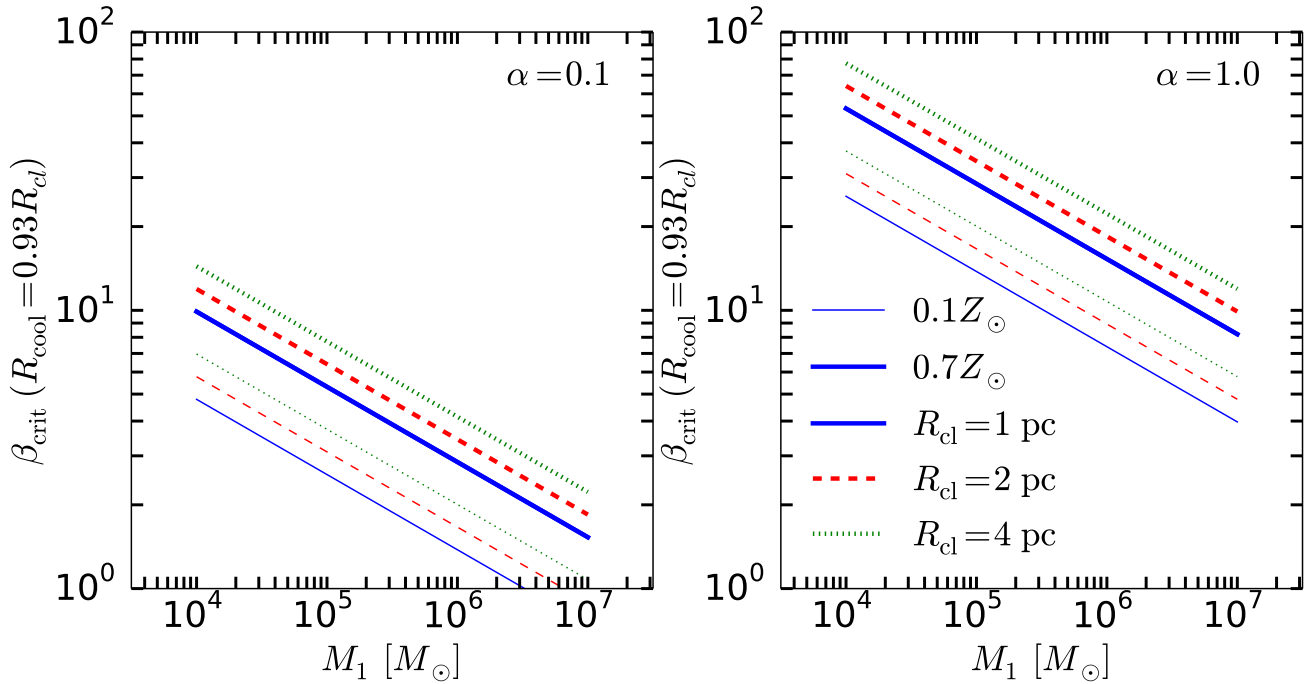


Figure 3. The critical value of mass-loading β required for the wind material deposited within 80% of the cluster volume to cool radiatively as a function of first generation stellar mass M_1 , for three cluster radii (blue solid for 1 pc, red dashed for 2 pc, green dotted for 4 pc), two cluster wind metallicities (heavy lines for $Z = 0.7Z_\odot$, thin lines for $Z = 0.1Z_\odot$), and two energy thermalization efficiencies ($\alpha = 0.1$ in left panel, $\alpha = 1$ in right panel).

tance of enrichment and dilution of He and other elements in §2.4 and §2.5.

For these reasons, we write the second generation stellar mass as

$$M_2 = (M_{\text{gas}} + \beta_{\text{wind}} M_w) \left(\frac{R_{\text{cool}}}{R_{\text{cl}}} \right)^3, \quad (18)$$

where β_{wind} is the mass enhancement factor for the wind only, and M_{gas} is the mass of ambient gas mixed with the wind material within the cluster, and is given by

$$M_{\text{gas}} = (\beta - \beta_{\text{wind}}) M_w, \quad (19)$$

where $M_w = \dot{M}_w \Delta t_{\text{SN}}$ is the mass of wind material that has accumulated in the cluster over the time Δt_{SN} , which is the time from the onset of strong mass deposition from winds at 2.5 Myr after formation until the first core-collapse supernova that does *not* collapse directly to a black hole occurs. Throughout the rest of this paper, we use $\Delta t_{\text{SN}} = 4.5$ Myr in our estimates, although the time until the first non-black-hole supernova is both uncertain (e.g. Pejcha & Thompson 2015; Sukhbold et al. 2016) and may be extended by rapidly rotating massive stars (Ekström et al. 2012). Although we scale to $\Delta t_{\text{SN}} = 4.5$ Myr throughout, in principle the second generation can form faster. Below we show that the cooling and freefall times are typically smaller than, but of order, $\Delta t_{\text{SN}} \sim 4.5$ Myr.

In this picture, $\beta_{\text{wind}} = 1$ corresponds to winds with \dot{M}_w given by equation (3), and $\beta > \beta_{\text{wind}}$ corresponds to mixing with ambient gas. In §2.4, we consider β_{wind} as large as ~ 3 , with a range of ambient gas masses from $\beta = \beta_{\text{wind}}$ (no mixing) to $\beta = 30 - 100$, where the latter values of β are

needed to match the second generation stellar mass fractions observed in globular clusters. For a given value of β_{wind} , equation (19) gives us a convenient way to represent the mass loading required to generate a given second generation stellar mass M_2 . In particular, we can quote both a mass loading parameter β and a corresponding mass of gas M_{gas} required to precipitate second generation formation of mass M_2 . Until §2.4, we consider only $\beta_{\text{wind}} = 1$.

If $\beta < \beta_{\text{crit, min}}$, then $M_2 = 0$ because none of the gas radiatively cools, and thus it all escapes the cluster. Figure 4 shows the critical M_{gas}/M_1 ratio required for cooling when $\beta_{\text{wind}} = 1$ at each fraction of the total cluster volume as the dashed curves for $\alpha = 0.1$ (thick) and $\alpha = 1$ (thin). The second generation mass that forms when M_{gas}/M_1 is equal to the critical value for cooling is the *minimum* value of M_2/M_1 (solid curves, thick for $\alpha = 0.1$ and thin for $\alpha = 1$). If $\beta > \beta_{\text{crit, min}}$ or, alternatively, if $M_{\text{gas}} > M_{\text{gas, crit}}$, the more massive the second generation will be. In order to have $M_2/M_1 \sim \text{few}$, we require $\beta \gg \beta_{\text{crit, min}}$ (thus $M_{\text{gas}}/M_1 \gg [M_{\text{gas}}/M_1]_{\text{crit}}$). For $(R_{\text{cool}}/R_{\text{cl}})^3 \sim 0.8$ and $M_{\text{gas}}/M_1 \sim 3$, $\beta \sim 100$. The $\alpha = 1$ $[M_{\text{gas}}/M_1]_{\text{crit}}$ curve falls above the $\alpha = 1$ $[M_2/M_1]_{\text{crit}}$ curve because more mass loading is necessary for the gas to cool when the energy thermalization efficiency is high, but not all of this gas enters into the second generation. Only a fraction $(R_{\text{cool}}/R_{\text{cl}})^3$ of the wind and ambient gas mixture forms the second generation.

For $\beta \sim 100$, the temperature of the thermalized gas is decreased by a factor of 100 (equation 9), which makes it $T \sim 8 \times 10^3$ K for $\alpha = 0.1$ and $T \sim 8 \times 10^4$ K for $\alpha = 1$. For $\alpha = 0.1$, the temperature is low enough that radiatively cooling will not lower the temperature further

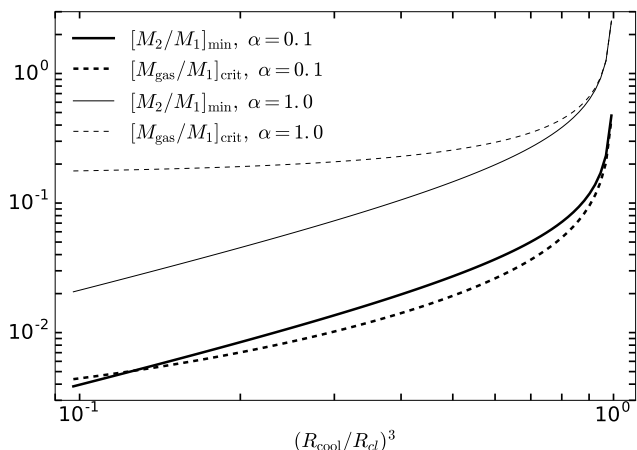


Figure 4. The critical minimum mass of ambient gas necessary for cooling $[M_{\text{gas}}/M_1]_{\text{crit}}$ (dashed) when $\beta_{\text{wind}} = 1$ and the resultant minimum second stellar generation mass at the critical ambient gas mass $[M_2/M_1]_{\text{min}}$ (solid) as a function of the fraction of the cluster’s volume that radiatively cools, $(R_{\text{cool}}/R_{\text{cl}})^3$. The model with efficiency of energy thermalization $\alpha = 0.1$ is shown with thick lines and the model with $\alpha = 1$ is shown with thin lines. If $M_{\text{gas}} = M_{\text{gas,crit}}$, then $M_2 = M_{2,\text{min}}$. If $M_{\text{gas}} > M_{\text{gas,crit}}$, then $M_2 > M_{2,\text{min}}$. The dashed curve corresponds to $\beta = \beta_{\text{crit}}$ in equation (19), and the solid curve corresponds to $M_{\text{gas}} = M_{\text{gas,crit}}$ in equation (18).

than the $\sim 10^4$ K photoionization maintains, so cooling is not necessary for winds to be retained in the cluster. For $\alpha = 1$, the temperature is in the low-temperature regime of the cooling function that scales as 0.3 with temperature for one-tenth solar metallicity, so equation (12) does not apply. However, our result that the thermalized gas radiatively cools is unchanged: a derivation of β_{crit} for this region of the cooling function gives $\beta_{\text{crit}} \sim 1$ for $T < 10^5$ K. $\beta \sim 100$ is far larger than this β_{crit} , so the thermalized gas in both cases of $\alpha = 0.1$ and $\alpha = 1$ will be cool enough to be retained within the cluster.

Radiative cooling is necessary, but not sufficient for the gas to form a second generation of stars. The massive stars in globular clusters output high fluxes of ionizing photons that, if the gas is not shielded, will maintain a temperature of $\sim 10^4$ K even in the cooled gas. Star formation requires cooler temperatures, so the radiatively cooled gas cannot be continuously ionized by the starlight in the cluster if a second stellar generation is to form (Palouš et al. 2014). Wünsch et al. (2017) show that the amount of mass that cools is consistently greater than the amount of mass necessary to shield a central clump of gas from the ionizing photons for $\alpha = 0.1$ ($\alpha = 1$ was not examined), thus allowing it cool below 10^4 K and form stars. We assume in our calculation that the amount of gas that cools is equal to the amount of gas that enters into the second generation. A model with smaller second generation star formation efficiencies will require proportionally more gas to produce a second stellar generation of a given size. Future numerical works should further assess this assumption and the ability of gas to self-shield.

Figure 5 shows the ratio of the stellar mass in the second generation to that in the first generation M_2/M_1 as a

function of the ratio of ambient gas mass to first-generation stellar mass within the cluster when $\beta_{\text{wind}} = 1$, for several cluster models with different first generation stellar masses. The upper edge limit of each curve corresponds to 80% of the cluster’s volume cooling ($R_{\text{cool}} = 0.93R_{\text{cl}}$ in equation 18), where $M_2/M_1 \propto M_{\text{gas}}/M_1$. The lower edge limit, where the curves end, corresponds to the inner 10% of the cluster volume ($R_{\text{cool}} = 0.46R_{\text{cl}}$). We avoid edge and center effects by focusing on 0.1 – 0.8 of the cluster’s volume (see discussion of equations 11, 12, and 13). Cooling and second generation star formation set in at lower M_{gas}/M_1 for higher M_1 because these GCs have a higher number density of massive stars depositing winds, and therefore do not require as much mass loading to reach the high densities necessary for radiative cooling. We explore other values of R_{cl} , but find our large- β results remain unchanged for $1 \text{ pc} < R_{\text{cl}} < 10 \text{ pc}$, so we focus on $R_{\text{cl}} = 1 \text{ pc}$ for the remainder of this paper.

The contours in Figure 6 show the ratio M_2/M_1 , as a function of both first generation stellar mass and ratio of ambient gas mass to first-generation stellar mass when $\beta_{\text{wind}} = 1$, for the same cluster models as in Figure 5. In order to produce a second stellar generation $\sim 0.5 - 3$ times the size of the first, a mass of ambient gas of order the mass of the first stellar generation or larger is required, regardless of the mass of the first generation. There is very little dependence of M_2/M_1 on the first-generation stellar mass of the cluster, as implied by all lines becoming vertical at large M_2/M_1 in Figure 6. Only M_{gas}/M_1 has much effect on M_2/M_1 in this limit. Certain combinations of M_1 and M_{gas} simply do not produce a second generation of stars at all, because the stellar winds combined with ambient gas never reach high enough density to raise the cooling rate above the heating rate ($\beta \lesssim \beta_{\text{crit,min}}$). This parameter space is the far left of the plot in the left panel, and pushes further to the right in the bottom of the right panel, where $\alpha = 1$. This is another visualization of the effect seen in Figure 5, where $\beta_{\text{crit,min}} \sim 5$ for $\alpha = 1$ implies that some amount of mass loading is always necessary for cooling to occur when the energy thermalization efficiency is high.

Figure 7 shows the formation time of the second generation as the sum of the cooling time and the free-fall time (calculated as $t_{\text{ff}} = \sqrt{3\pi/(32G\mu m_p n)}$ with density n given by equation 7) as a function of M_{gas}/M_1 for the same cluster models from Figures 5 and 6⁴. We assume the first generation forms instantaneously, but that significant post-main sequence massive star winds do not turn on until 2.5 Myr. The cooling time is given by

$$t_{\text{cool}} = \frac{3}{2} \frac{P}{\Gamma_{\text{cool}}} \quad (20)$$

where P is the pressure of the thermalized wind ejecta and ambient gas mixture.

The horizontal gray band at 3–5 Myr in Figure 7 shows the approximate time after the onset of winds at 2.5 Myr when the first supernova from the most massive star in the first generation can be expected to occur 3–5 Myr after star

⁴ We calculate t_{ff} assuming constant density within R_{cool} , but the shock-compressed cooling gas can have much higher density and lower free-fall time. This would allow the second generation to form faster than we predict, and thus our estimates are upper limits on the time to form a second generation.

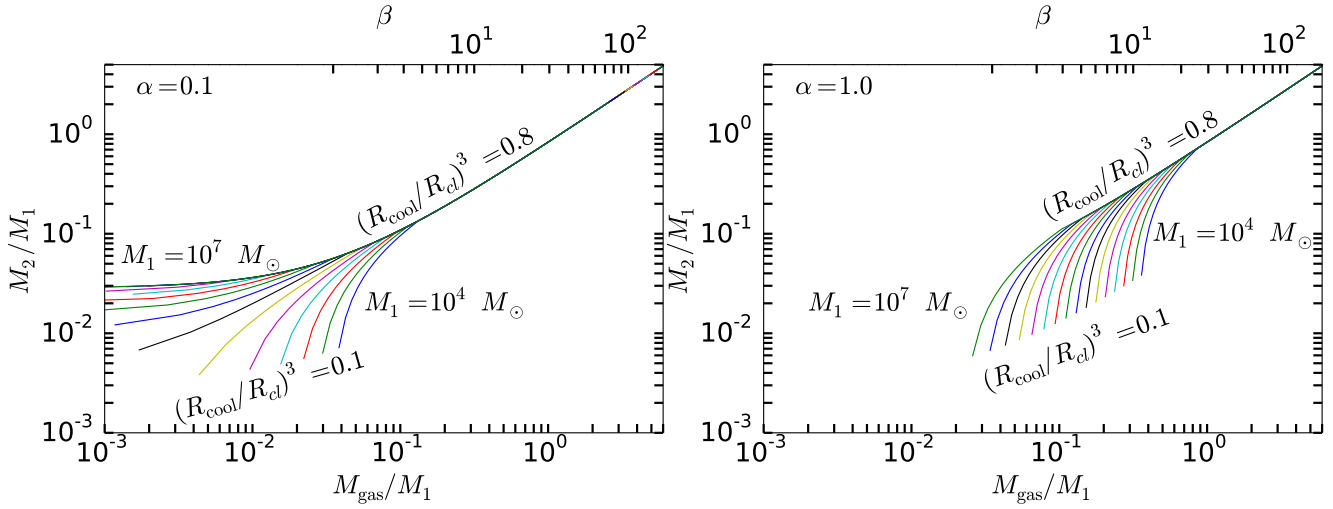


Figure 5. The ratio of the second generation’s stellar mass M_2 to the first generation’s stellar mass M_1 as a function of the ratio of ambient gas mass M_{gas} to the first generation stellar mass when $\beta_{\text{wind}} = 1$. Curves show different first generation masses, from $10^4 M_{\odot}$ to $10^7 M_{\odot}$, in multiples of $10^{0.2}$. Left panel shows models with energy thermalization efficiency $\alpha = 0.1$ and right panel shows models with $\alpha = 1$. All GCs have radius $R_{cl} = 1$ pc, one-tenth solar metallicity, and have been accumulating wind material for $\Delta t_{\text{SN}} = 4.5$ Myr. Top axis shows β values corresponding to M_{gas}/M_1 values on bottom axis.

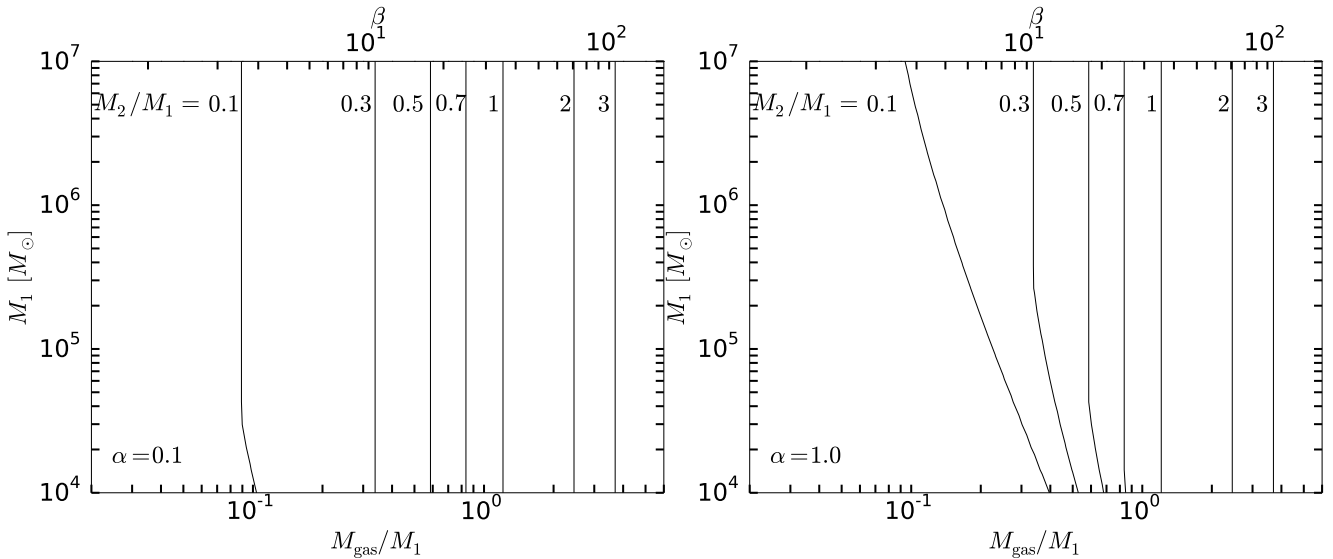


Figure 6. Contour plot of the ratio of stellar mass in the second generation to the first generation, M_2/M_1 , as a function of both the first generation stellar mass M_1 and ratio of gas mass to first generation stellar mass, M_{gas}/M_1 , when $\beta_{\text{wind}} = 1$. Models in left panel have energy thermalization efficiency $\alpha = 0.1$ and models in right panel have $\alpha = 1$. All clusters shown here have radius $R_{cl} = 1$ pc, one-tenth solar metallicity, and have been accumulating wind material for $t_{\text{SN}} = 4.5$ Myr. Top axis shows β values corresponding to M_{gas}/M_1 values on bottom axis.

formation, when the winds turn on. For the more massive clusters, $t_{\text{cool}} + t_{\text{ff}} < 3$ Myr for all M_{gas}/M_1 , justifying that star formation can occur rapidly, before supernovae. The “kink” in the curves is where $(R_{\text{cool}}/R_{cl})^3 = 0.8$, where the cooling radius is then held constant instead of increasing further toward R_{cl} . Any values of M_{gas}/M_1 greater than this point for a given curve have $M_{\text{gas}}/M_1 > [M_{\text{gas}}/M_1]_{\text{crit}}$, and we see that larger values of M_{gas}/M_1 reduce $t_{\text{cool}} + t_{\text{ff}}$ below 3 Myr for all clusters. Note that parameter regimes with $t_{\text{ff}} +$

$t_{\text{cool}} > \Delta t_{\text{SN}}$ would either occur in low mass clusters or when M_{gas}/M_1 is small enough that it will not produce a sizable second generation. For $\alpha = 1$, very few combinations of M_1 and M_{gas}/M_1 do not cool and collapse before supernovae begin because $M_{\text{gas}}/M_1 \sim 1$ is necessary for cooling to occur at all, so if cooling does occur, there is a high gas density and the free fall and cooling times are short. For our fiducial GC with $M_1 = 10^5 M_{\odot}$, $R_{cl} = 1$ pc, $\alpha = 0.1$, and one-tenth solar metallicity, Figure 6 shows $M_{\text{gas}}/M_1 \sim 0.5 - 4$ is necessary

to form a second generation 0.5 – 3 times as massive as the first when $\beta_{\text{wind}} = 1$. This means our fiducial cluster would form a second generation in $t_{\text{cool}} + t_{\text{ff}} \approx 1 - 3$ Myr — before core collapse supernovae begin.

2.3 Comparison with Observations

With an understanding of how the various GC parameters affect the mass of the second generation of stars, we can now compare our model to observations of multiple stellar generations in GCs. Several studies (e.g. Carretta et al. 2011, 2014; Gratton et al. 2015; Milone et al. 2017) have examined the spread of light element abundances in Galactic GCs to determine which stars are members of first and second stellar generations. The ratio of second generation to first generation stars can be as low as $M_2/M_1 \sim 0.35$ (Boberg et al. 2016) or $M_2/M_1 \sim 0.5$ (Milone et al. 2017), but are more typically $M_2/M_1 \sim 2 - 3$ (Carretta et al. 2009a). Using the GC masses and half-light radii from the database presented in McLaughlin & van der Marel (2005) and the first generation fractions from Carretta et al. (2009a); Niederhofer et al. (2016a,b); Milone et al. (2017), we plot M_1/R_h as a function of M_1 in Figure 8 as the dark, solid points, where M_1 is the stellar mass of the first generation and R_h is the half-light radius. We assume that the initial mass functions of both generations are equivalent and well-sampled so that the fraction of stars in each generation is equivalent to the fraction of initial stellar mass in each generation. The open points are clusters that were identified as being only-first generation or mostly-first generation by Caloi & D’Antona (2011), but we plot only those clusters in their sample that were *not* later found to be hosting multiple populations: NGC 6235, AM 1, ARP 2, PAL 3, PAL 4, and PAL 14. The light gray solid points are all other clusters in the McLaughlin & van der Marel (2005) database. Lines connecting dark solid points indicate that multiple studies examined a particular cluster and determined different values for the first generation fraction, thus giving different values of M_1 for the same cluster. With the exception of a few outliers, it seems that those clusters that are made of only- or mostly-first generation stars have lower values of M_1/R_h at all M_1 than those clusters with an identified second generation.

Figure 8 also shows the critical condition on M_1/R_{cl} for nearly all of the cluster’s volume to cool (see equation 15), for a few different values of α and β , as the solid, dashed, and dotted lines. If a cluster has the specified values of α and β , then our model predicts it would form a second generation if it falls above the line, and would not if it falls below the line. The location of the model lines in this plot are highly sensitive to the choice of α and β , which are not observationally well-constrained. The dotted line, which shows $[M_1/R_{cl}]_{\text{crit}}$ for $\alpha = 0.1$ and $\beta = 25$, splits the clusters into those with measured second generation fractions and those that are only or mostly first generation. Our model predicts that a cluster with these parameters would produce a second generation of mass $M_2 \sim 0.7M_1$ if its M_1/R_{cl} falls above this line.

Comparing the model lines to the data in Figure 8 has several caveats. First, we have assumed that R_{cl} , the radius within which the first generation’s massive stars deposit their winds, is equal to the observed half-light radius R_h , but the first generation massive stars could have been centrally-

concentrated. Second, the fraction of second generation stars is not well-constrained, as different methods for separating the two generations yield sometimes different fractions, and this changes where a cluster falls in this figure because it directly affects M_1 . For example, NGC 6809 was found to have a first generation fraction of $M_1/(M_1 + M_2) \approx 0.20 \pm 0.05$ by examining the sodium-oxygen anticorrelation by Carretta et al. (2009a), and $M_1/(M_1 + M_2) \approx 0.311 \pm 0.029$ by examining the split red giant branch in a two-color map by Milone et al. (2017). Third, our model’s predictions are strongly dependent on the values of α and β , which may vary from cluster to cluster with ambient gas mass, metallicity, or cluster environment.

Importantly, most clusters where the second generation has been studied are high-mass. Figure 9 and the critical condition of equation (15) imply that a cluster with low M_1/R_{cl} cannot form a second generation because the winds do not meet the critical condition for radiative cooling and retention of the wind material. Verifying any mass dependence of the presence of a second generation requires studying low-mass clusters as well.

Figure 9 shows the ratio of mass in the second stellar generation to that in the first for the same clusters indicated by the dark solid points in Figure 8 and values of M_2/M_1 for different values of M_{gas}/M_1 when $\beta_{\text{wind}} = 1$ (right vertical axis), as functions of M_1 . There is no variation in our model with M_1 for the values of M_{gas}/M_1 shown (see Figure 6) for $\alpha = 0.1$, and only some variation for the lower values of M_2/M_1 for $\alpha = 1$, and there is also little variation in M_2/M_1 with M_1 in the data. Points and connecting lines have the same meaning as in Figure 9.

In order to produce a second generation 0.5 – 3 times as large as the first, $M_{\text{gas}}/M_1 = 0.5 - 4$ is necessary if $\beta_{\text{wind}} = 1$. For this range of M_{gas}/M_1 of our fiducial cluster ($M_1 = 10^5 M_{\odot}$), the final mass after the second generation has formed is $M_1 + M_2 = 1.5 - 5.5 \times 10^5 M_{\odot}$. If post-main sequence wind mass loss rates are enhanced ($\beta_{\text{wind}} > 1$), the ambient gas mass required to form a second generation comparable in mass to the first is less than the ambient gas mass required when $\beta_{\text{wind}} = 1$.

2.4 Helium Abundances

We now turn to the light-element abundance spreads of GCs, focusing on the helium enrichment of the second generation. Since our model thus far does not include abundance information beyond an overall metallicity, we adopt a model for wind ejecta from massive stars. We use the pre-supernova wind abundances for non-rotating solar metallicity stars from the recent core-collapse simulations of Sukhbold et al. (2016). Because GC $[\text{Fe}/\text{H}]$ values are -2 to -1 we assume the metallicity of the stars does not have a very strong effect on the relative helium content of the winds for the purposes of our estimate.

As winds from the most massive stars dominate the mass and energy deposition at early times in GCs, we focus on stars with masses 25 – 120 M_{\odot} . Sukhbold et al. (2016) calculate wind abundances for many stellar masses in the range 25 – 120 M_{\odot} , within which we linearly interpolate to obtain a finer stellar mass sampling. We integrate wind masses with a Salpeter IMF to obtain the total mass in winds produced by stars in our selected mass range. The

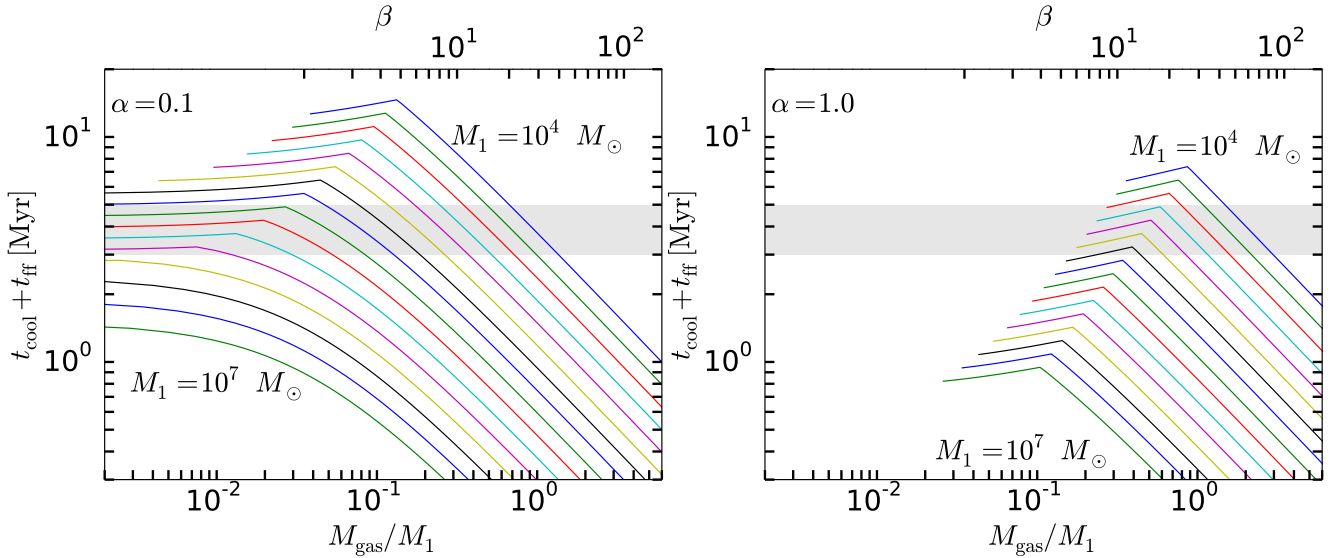


Figure 7. The sum of the cooling time and the free fall time for GCs with first generations in the mass range $10^4 M_\odot$ to $10^7 M_\odot$, in multiples of $10^{0.2}$, as a function of the ratio of ambient gas to first generation stellar mass when $\beta_{\text{wind}} = 1$. Left panel shows models with energy thermalization efficiency $\alpha = 0.1$ and right panel shows models with $\alpha = 1$. These are all clusters with $R_{\text{cl}} = 1$ pc, $Z = 0.1Z_\odot$, and they have been accumulating material from stellar winds for $\Delta t_{\text{SN}} = 4.5$ Myr. Horizontal gray band at 3–5 Myr shows the approximate time after winds turn on at which the most massive stars end their lives *without* direct collapse to black hole. Top axis shows values of β that correspond to values of M_{gas}/M_1 on bottom axis.

IMF-integrated wind mass from [Sukhbold et al. \(2016\)](#) is not equal to the mass in winds, M_w , from STARBURST99, so we multiply the [Sukhbold et al. \(2016\)](#) yields by a correction factor of ~ 0.75 .

We calculate $\Delta Y = \Delta \frac{M_{\text{He}}}{M_{\text{tot}}}$ as

$$\Delta Y = \frac{M_{\text{He,wind}} + M_{\text{He,gas}}}{M_{\text{wind}} + M_{\text{gas}}} - Y_1, \quad (21)$$

where $M_{\text{He,wind}}$ is the mass of helium in the wind, $M_{\text{He,gas}}$ is the mass of helium in the ambient gas, M_{wind} is the total mass of wind, and Y_1 is the Y value of the first stellar generation. The first stellar generation has

$$Y_1 = \frac{M_{\text{He},\odot}}{M_{\text{H},\odot} + M_{\text{He},\odot} + Z_{\text{gas}} \times M_{\text{metals},\odot}}, \quad (22)$$

where $(M_{\text{He},\odot}/M_{\text{H},\odot}) \simeq 0.382$ and $(M_{\text{metals},\odot}/M_{\text{H},\odot}) \simeq 0.02$. For a gas metallicity of one-tenth solar, $Y_1 \simeq 0.276$. Since the ambient gas has the same elemental make-up as the first generation, this means $Y_{\text{gas}} = M_{\text{He,gas}}/M_{\text{gas}} \simeq 0.276$ as well. We find $M_{\text{He,wind}}$ and M_{wind} from the yields produced by [Sukhbold et al. \(2016\)](#).

Using equation (19), if $\beta_{\text{wind}} = 1$, then

$$\begin{aligned} \Delta Y &= \frac{M_{\text{He,wind}} + Y_{\text{gas}} \dot{M}_w \Delta t_{\text{SN}} (\beta - 1)}{\dot{M}_w \Delta t_{\text{SN}} + \dot{M}_w \Delta t_{\text{SN}} (\beta - 1)} - Y_1 \\ &= \frac{Y_{\text{wind}} + Y_{\text{gas}} (\beta - 1)}{\beta} - Y_1 \end{aligned} \quad (23)$$

where $Y_{\text{wind}} = M_{\text{He,wind}}/M_{\text{wind}}$. All dependence on first generation stellar mass drops out because $M_{\text{He,wind}} \propto M_1$ and $M_{\text{wind}} \propto M_1$. However, there is still dependence of ΔY on the total mass of the cluster, $M_1 + M_2$, because a higher β indicates a higher M_{gas} , which increases M_2 (see eq. 18). If $\beta_{\text{wind}} > 1$, we use equation (19) to write β in terms of β_{wind} ,

$\dot{M}_w \Delta t_{\text{SN}}$, and M_{gas} , and find

$$\begin{aligned} \Delta Y &= \frac{(Y_{\text{wind}} - Y_{\text{gas}}) (R_{\text{cool}}/R_{\text{cl}})^3 \beta_{\text{wind}} \dot{M}_w \Delta t_{\text{SN}} M_1^{-1}}{M_2/M_1} - Y_1 \\ &\approx 0.015 \beta_{\text{wind},3} \left(\frac{M_1}{M_2} \right) \left(\frac{\dot{M}_w}{10^{-3.1} M_\odot \text{ yr}^{-1}} \right) \\ &\times \left(\frac{R_{\text{cool}}/R_{\text{cl}}}{0.93} \right)^3 \left(\frac{\Delta t_{\text{SN}}}{4.5 \text{ Myr}} \right) \left(\frac{M_1}{10^5 M_\odot} \right)^{-1} \end{aligned} \quad (24)$$

where we have assumed $Y_{\text{gas}} = Y_1 = 0.276$ and $Y_{\text{wind}} = 0.44$, and scaled to $\beta_{\text{wind}} = 3$, the maximum mass enhancement of the wind (see below). Equation (24) only holds for $M_2 \geq \beta_{\text{wind}} M_{\text{wind}}$, and ΔY is maximum when $M_2 = \beta_{\text{wind}} M_{\text{wind}}$ (see below).

Figure 10 shows ΔY in equation (24) as a function of the ratio of second generation to first generation mass, for our fiducial massive star winds \dot{M}_w when $\beta_{\text{wind}} = 1$ as the solid line. Producing a larger value of M_2/M_1 requires a larger amount of ambient gas, which dilutes the wind material and yields lower values of ΔY . The helium enhancement is $\Delta Y \sim 0.002 - 0.013$ for $M_2/M_1 \sim 0.5 - 3$, which is produced by mixing with $M_{\text{gas}}/M_1 \sim 0.5 - 4$.

Milky Way GCs have inferred helium enhancements of $\Delta Y \sim 0.01 - 0.04$, with some as high as $\Delta Y \sim 0.08$ or as low as $\Delta Y \sim 0.001$, but these values are uncertain ([MacLean et al. 2016](#); [Valcarce et al. 2014](#)). [Bastian et al. \(2015\)](#) show no theoretical models can self-consistently produce all aspects of elemental abundance differences because there is a wide spread of helium enhancement among GCs, and we find our model cannot produce both inferred ΔY values and measured M_2/M_1 values for GCs (shown as black points in Figure 10).

If the wind material does not mix with any ambient gas, ΔY for the second generation is equal to that of stellar winds

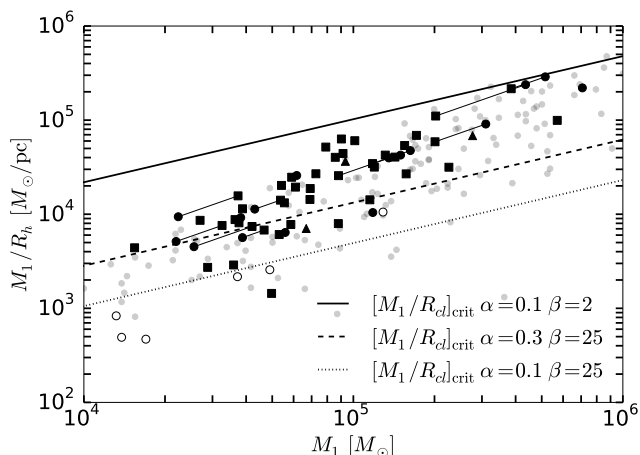


Figure 8. The ratio of mass in the first stellar generation M_1 to the cluster’s half-light radius R_h as a function of M_1 . Solid, dark points indicate clusters where a second stellar generation has been identified: circles are clusters from Carretta et al. (2009a), squares are clusters from Milone et al. (2017), and triangles are clusters from Niederhofer et al. (2016a,b). Open circles are clusters that are identified as candidates for only first generation or mostly first generation by Caloi & D’Antona (2011). Light gray solid circles are all other clusters in the McLaughlin & van der Marel (2005) database not included in the aforementioned six studies, for which we assume the first generation stellar mass is equal to the total stellar mass of the cluster for the purposes of plotting. Lines connecting solid dark points indicate that the multiple points represent a single cluster for which different studies found different first generation fractions. Solid, dashed, and dotted lines show the minimum value of M_1/R_{cl} a cluster must have for nearly all of it to cool and form a second generation, for three combinations of α and β (see equation 15), where we assume $R_{cl} = R_h$ (see caveats in text).

alone. The winds have a very high helium enhancement, $\Delta Y \approx 0.16$, higher than most observed GCs. ω Cen has an anomalously high helium enrichment value typically not seen in other GCs, $\Delta Y = 0.14$ (Piotto et al. 2005). However, without mixing with ambient gas, a second generation with mass comparable to the first generation cannot form. In addition, dilution with pristine, ambient gas is required to reproduce observed elemental abundance variations (D’Ercole et al. 2011, see §2.5 below) and lithium content (Prantzos & Charbonnel 2006). We can produce somewhat higher second generation helium enhancements by enhancing the wind mass loss rates over our reference value of \dot{M}_w (equation 3), but still require some mixing with ambient gas. For example, if $\beta_{wind} \sim 2$, making \dot{M}_w 2 times larger than our reference value in equation (3), then the winds would need to mix with $M_{gas}/M_1 \sim 0.76$ to produce $\Delta Y \sim 0.02$ (a typical value of ΔY for MW GCs) and also produce a second generation of size $M_2/M_1 \sim 0.6$, consistent with the lowest observed values of M_2/M_1 .

We can estimate an upper bound on the mass of wind material deposited by post-main sequence massive stars by assuming that all mass lost between the zero-age main sequence (ZAMS) mass of the star and its pre-supernova mass is deposited as winds during $\Delta t_{SN} \approx 4.5$ Myr. Since most of a massive star’s wind material will be deposited near the end of its lifetime, those stars with masses less than

$25M_\odot$ (the lowest mass star that does not collapse directly to black hole in our model) will not deposit all of their wind mass during Δt_{SN} , but assuming that they do provides an effective upper limit on β_{wind} , and thus \dot{M}_w . We calculate this total mass loss as the difference between the ZAMS mass and final pre-supernova mass from Table 2 of Sukhbold et al. (2016), which gives the pre-supernova mass of all stars in the 9 – 120 M_\odot range. Dividing this sum of material by $\Delta t_{SN} = 4.5$ Myr, the time between massive star winds “turn on” and the first supernova, when we assume winds are most active, gives a value for a maximum mass deposition rate of

$$\dot{M}_{w,max} = 10^{-2.7} M_\odot \text{ yr}^{-1} \left(\frac{M_1}{10^5 M_\odot} \right), \quad (25)$$

which is ~ 2.5 times higher than our reference value of \dot{M}_w in equation (3), implying $\beta_{wind,max} \sim 2.5$.⁵

For $\dot{M}_{w,max}$, $\beta_{crit,max} \sim 0.8$, so no mass loading at all is necessary for a significant volume of the wind material to cool. However, producing a second generation mass ~ 0.5 –3 times the first generation requires a mass-loading value of $\beta \sim 7$ –40, compared to $\beta \sim 20$ –100 for our reference value of \dot{M}_w in equation (3). Because $\dot{M}_{w,max}$ is an estimate for the maximum mass deposition the wind can have, we interpret additional mass loading as mixing with ambient gas. Mass-loading of $\beta \sim 7$ –40 corresponds to masses of ambient gas $M_{gas}/M_1 \sim 0.5$ –3.7, compared to $M_{gas}/M_1 \sim 0.5$ –4 when $\beta_{wind} = 1$.

Increasing \dot{M}_w to $\dot{M}_{w,max}$ has a small effect on the mass of ambient gas required because the amount of total mass in the second generation is dominated by ambient gas mass. However, there is a strong effect on abundances. Figure 10 shows ΔY for models with \dot{M}_{max} as a function of M_2/M_1 as the dashed line. Increasing \dot{M}_w to \dot{M}_{max} changes ΔY from ~ 0.002 –0.013 in our fiducial model to $\Delta Y \sim 0.004$ –0.023. Since no ambient gas mixing is necessary for cooling for \dot{M}_{max} , ΔY could be as high as $Y_{wind} - Y_1 \approx 0.16$ if the wind material does not mix with any ambient gas, but without any mass loading, the wind alone would only form a second generation of size $M_2/M_1 \sim 0.06$. To produce a helium enhancement of $\Delta Y \sim 0.02$, the winds could mix with an amount of ambient gas $M_{gas}/M_1 \sim 0.66$, which would produce a second generation of size $M_2/M_1 \sim 0.6$. Even $\dot{M}_{w,max}$ cannot produce both helium enhancements larger than $\Delta Y \sim 0.025$ and a second generation larger than $M_2/M_1 \sim 0.5$.

We make a final estimate for the maximum amount of helium that could in principle be ejected before supernovae set in by imagining that all stars lose their hydrogen and helium envelopes before explosion. We estimate the helium envelope mass from the models of Woosley & Weaver (1995), who calculated the evolution and explosion of massive stars.

⁵ Our $\dot{M}_{w,max}$ is ~ 0.2 dex lower than the implied mass loss rate from de Mink et al. (2009) for massive binaries, if we assume their reported total wind mass of 13% of the first generation stellar mass is entirely deposited during Δt_{SN} , before supernovae. Our value is lower because we calculate the wind mass as the difference between the initial stellar mass and the pre-supernova stellar mass, and de Mink et al. (2009) calculate the difference between the initial stellar mass and the (post-supernova) remnant mass.

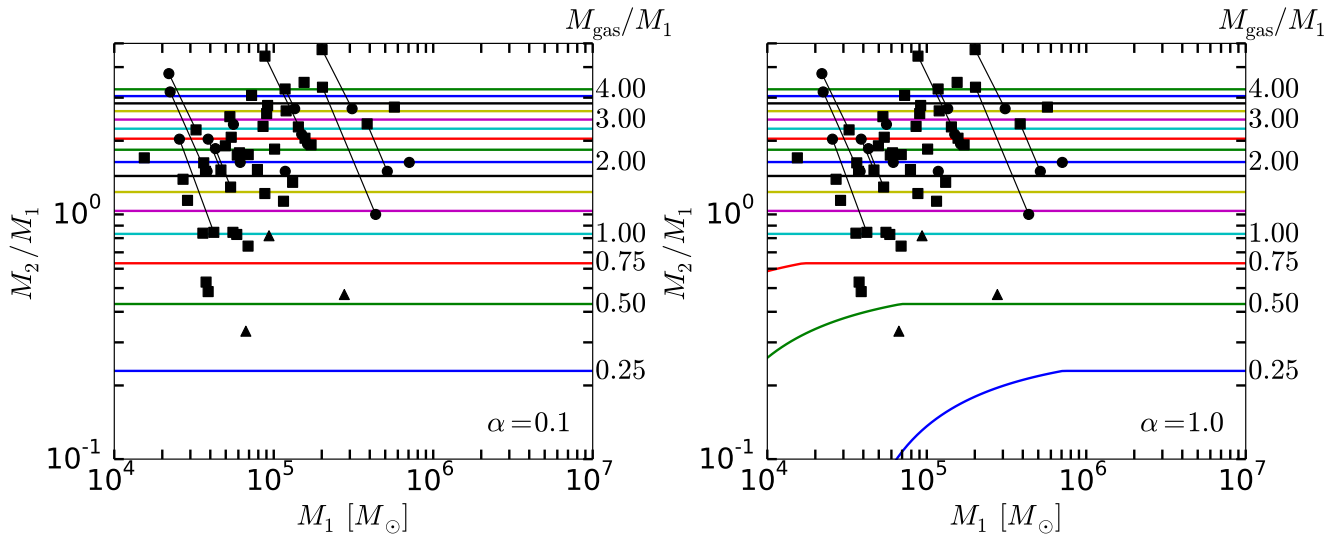


Figure 9. Colored lines indicate the ratio of second generation stellar mass to first generation stellar mass in our fiducial model as a function of first generation stellar mass. Left panel shows models with energy thermalization efficiency $\alpha = 0.1$, and right panel shows models with $\alpha = 1$. M_2/M_1 increases from $M_2/M_1 \sim 0.2$ to $M_2/M_1 \sim 3$ as M_{gas}/M_1 increases from 0.25 to 4 when $\beta_{\text{wind}} = 1$, as indicated by labels for select curves to right of plot. Filled circles are clusters examined by Carretta et al. (2009a), filled squares are those examined by Milone et al. (2017), and filled triangles are those examined by Niederhofer et al. (2016a,b). Lines connecting points indicate where a cluster was found by different studies to have different first generation fractions, thus changing both M_1 and M_2/M_1 for that cluster. Curves were produced by our model with one-tenth solar metallicity and have accumulation of wind material for $\Delta t_{\text{SN}} = 4.5$ Myr.

Roughly $\sim 1/3$ of the ZAMS mass is contained in the helium shell and $\sim 1/3$ in the hydrogen shell. Integrating over the IMF, we find a maximum allowed mass lost in winds if all massive stars eventually collapse as bare cores, with successful explosions producing Type Ic supernovae. Assuming all of this mass is ejected during Δt_{SN} produces a mass loss rate of $\dot{M}_{\text{WW95}} \sim 10^{-2.5} M_{\odot} \text{ yr}^{-1}$ for a cluster of mass $10^5 M_{\odot}$. The dot-dashed line in Figure 10 shows the relation between ΔY and M_2/M_1 resulting from a wind mass loss rate of $\dot{M}_{\text{WW95}} \sim 10^{-2.5} M_{\odot} \text{ yr}^{-1}$ where half of the ejected wind mass is helium. This relation still underpredicts the inferred ΔY and M_2/M_1 of observed GCs.

To reproduce the GC ΔY data, our model would need a wind mass loss rate of $\dot{M} \sim 10^{-2} M_{\odot} \text{ yr}^{-1}$ (shown as dotted line in Figure 10), larger than our simple estimate for the maximum mass loss rate a GC could have. Such a mass-loss rate would imply 45% of the first stellar generation’s mass is ejected in winds, ~ 12 times larger than our fiducial \dot{M}_w , ~ 5 times larger than $\dot{M}_{w,\text{max}}$ in equation (25), and ~ 3 times larger than \dot{M}_{WW} derived above, and would require a flatter high-mass IMF than we have assumed. This emphasizes the problem of all self-enrichment models, including our own, where there is not enough wind material available to produce a large enough second generation with large enough elemental enhancements. We emphasize that while the helium enhancement (Milone 2015) and second generation fraction (Milone et al. 2017) are both seen to increase with GC mass, we do not find a strong correlation or anti-correlation between ΔY and M_2/M_1 for clusters reported in the literature. If such an anti-correlation is established, it would provide evidence for the self-enrichment scenario. For all but one of the observed GCs plotted in Figure 10, our models, including the one with a maximum mass loss

rate that we estimate a GC could have, underestimate either the reported ΔY values or the reported M_2/M_1 values for literature GCs.

We can calculate a ΔZ analogous to our calculation of ΔY , where instead of using the helium mass content of the wind material, we sum the mass content of all elements heavier than helium in the wind. Regardless of the fraction of wind material in the mixture of ambient gas and wind material, $\Delta Y/\Delta Z \sim 1.6$ in our model. This does not depend on M_{gas} because ΔY and ΔZ depend on M_{gas} in the same way, so all M_{gas} dependence drops out in the ratio $\Delta Y/\Delta Z$.

Because the time for the second generation of stars to form, $\Delta t_{2\text{gen}} = t_{\text{ff}} + t_{\text{cool}}$ (see Figure 7), is shorter than the time Δt_{SN} when the first supernova that does not collapse directly to black hole occurs, it is possible for the second generation to form before massive star winds have deposited very much of their mass into the cluster. We assumed above that all of the wind material massive stars deposit over their entire post-main sequence evolution enters into the second stellar generation, when more precisely the amount of wind material in the second generation would be given by $M_w = \dot{M}_w \Delta t_{2\text{gen}}$ when $\beta_{\text{wind}} = 1$. This would create a second generation that is even more diluted by ambient gas than what we derive above, because $\Delta t_{2\text{gen}} \lesssim \Delta t_{\text{SN}}$. Even under the assumption that $\Delta t_{2\text{gen}} \sim \Delta t_{\text{SN}}$, the second generation mass is dominated by the ambient gas mass, so $\Delta t_{2\text{gen}} < \Delta t_{\text{SN}}$ does not have a large impact on the amount of ambient gas required to form a large second generation — $M_{\text{gas}}/M_1 \sim 1.24$ to produce $M_2/M_1 \sim 1$ for $\Delta t_{2\text{gen}} \sim 1$ Myr, compared to $M_{\text{gas}}/M_1 \sim 1.21$ to produce the same M_2/M_1 under the assumption $\Delta t_{2\text{gen}} \sim \Delta t_{\text{SN}} \sim 4.5$ Myr. However, the difference in the value of β required to produce $M_2/M_1 \sim 1$ is quite large, $\beta \sim 157$ for $\Delta t_{2\text{gen}} \sim 1$ Myr, com-

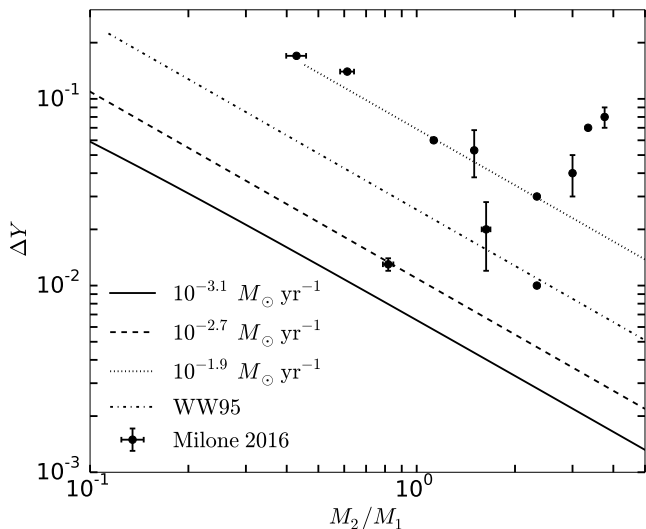


Figure 10. The helium enrichment of second generation stars relative to first generation stars as a function of the ratio of second generation mass to first generation mass (equation 24). The solid line gives the relation for our fiducial cluster with $\beta_{\text{wind}} = 1$, $\dot{M}_w = 10^{-3.1} M_{\odot} \text{ yr}^{-1}$, $M_1 = 10^5 M_{\odot}$, $R_{cl} = 1 \text{ pc}$, $Z = 0.1 Z_{\odot}$, $\alpha = 0.1$, and $\Delta t_{\text{SN}} = 4.5 \text{ Myr}$. The dashed line gives the relation for a similar cluster with $\beta_{\text{wind}} \sim 2.5$, which gives $\dot{M}_{\text{max}} = 10^{-2.7} M_{\odot} \text{ yr}^{-1}$. The black points are inferred values of ΔY and measured M_2/M_1 for a handful of clusters presented in Milone (2015) (see their Figure 10), the dotted line is our relation for a cluster with $\dot{M} = 10^{-1.9} M_{\odot} \text{ yr}^{-1}$, and the dot-dashed line is the relation for a cluster with He ejecta values from Woosley & Weaver (1995). Typical quoted errors on M_2/M_1 are $\sim 3\%$, and we plot values of ΔY with their quoted errors. Note the dotted line is not a fit to the data.

pared to $\beta \sim 35$ in our fiducial model, which means the difference in ΔY is also large: $\Delta Y \sim 0.001$ for $\Delta t_{2\text{gen}} \sim 1 \text{ Myr}$ compared to $\Delta Y \sim 0.005$ for our fiducial model. Shortening $\Delta t_{2\text{gen}}$ thus has a large impact on the second generation abundances, but not on the mass of ambient gas required to produce a large second generation. Because $\Delta t_{2\text{gen}}$ and Δt_{SN} are of the same order of magnitude, we scale $\Delta t_{2\text{gen}}$ to Δt_{SN} as a reference, but note that the precise value of $\Delta t_{2\text{gen}}$ impacts ΔY .

2.5 Other Light Element Abundances

In observed GCs, the variations in light element abundances determine which stars are classified as members of the first or second generations. The most notable light-element spread is the sodium-oxygen anticorrelation, in which second generation stars are Na-enriched and O-poor, whereas first-generation stars are O-enriched and Na-poor. The ~ 1235 red giant stars across the 19 GCs in the C09 sample have a spread from $[\text{O}/\text{Fe}] \sim 0.0 - 0.7$ and $[\text{Na}/\text{Fe}] \sim -0.4 - 0.0$ for the first generation and $[\text{O}/\text{Fe}] \sim -0.7 - 0.5$ and $[\text{Na}/\text{Fe}] \sim 0.0 - 1.0$ for the second generation across all GCs studied. The iron abundances are equivalent across generations for most observed GCs, so we will focus on $[\text{O}/\text{Na}]$. For the first generation, $[\text{O}/\text{Na}] \sim 0.0 - 1.0$ and for the second generation, $[\text{O}/\text{Na}] \sim -1.5 - 0.5$.

We analyzed the oxygen and sodium yields for the wind

material in the Sukhbold et al. (2016) models, and found that the winds of stars in the mass range $30 M_{\odot} < M < 120 M_{\odot}$ have spreads of $[\text{O}/\text{Na}] \sim -0.2 - 0.4$. Because our model assumes complete mixing of winds from all stellar masses, there is no spread in abundances in the second generation. However, we can approximate a type of incomplete mixing if we instead assume winds from the most massive stars form the first of the second generation stars and winds from the least massive stars form the last of the second generation. There would then be a spread in abundances within the second stellar generation because winds from different mass stars have different abundances. Note that this method of producing a spread in abundances still will not produce as large of an abundance spread as allowing wind material to be diluted to various degrees with ambient gas. If the second generation of stars is entirely made out of wind material, with no mixing with pristine ambient gas at all, then the wind abundances would exactly represent the abundances for the second generation in our model (but the second generation would be small). The spread in $[\text{O}/\text{Na}]$ is not as wide as the observed spread in second generations, because we do not include variable mixing of wind material with ambient gas.

To create a second stellar generation 0.5 – 3 times more massive than the first, mixing with a mass of ambient gas $M_{\text{gas}}/M_1 \sim 0.5 - 4$ is necessary for our reference value of \dot{M}_w ($\beta_{\text{wind}} = 1$). We assume the ambient gas and first stellar generation have one-tenth solar Fe abundances, and use $[\text{O}/\text{Fe}] \sim 0.35$ and $[\text{Na}/\text{Fe}] \sim -0.1$ for the ambient gas, to match the oxygen and sodium abundances of the first stellar generation. After mixing, the wind abundances are diluted by the ambient gas, so the spread in abundances of the second generation becomes $[\text{O}/\text{Na}] \sim -0.1 - 0.4$ for $M_{\text{gas}}/M_1 \sim 0.5$ and $[\text{O}/\text{Na}] \sim 0.18 - 0.45$ for $M_{\text{gas}}/M_1 \sim 4$. When mixing with such a large mass of ambient gas, the second generation abundances do not match the spread of the observed second generation abundances, but the values of $[\text{O}/\text{Na}]$ are still consistent with the second generation.

If we increase \dot{M}_w to $\dot{M}_{\text{max}} = 10^{-2.7} M_{\odot} \text{ yr}^{-1}$, a somewhat smaller value of $M_{\text{gas}}/M_1 \sim 0.5 - 3.7$ is necessary to produce a second generation ratio $M_2/M_1 \sim 0.5 - 3$. The value of $[\text{O}/\text{Na}]$ for the winds alone without mixing are the same for \dot{M}_{max} as they are for \dot{M}_w because increasing the overall magnitude of the wind does not change its relative abundances. However, using \dot{M}_{max} does change the relative amounts of wind material and ambient gas in the mixture, so the spreads in $[\text{O}/\text{Na}]$ are different than for \dot{M}_w when mixing with various amounts of ambient gas. For $M_{\text{gas}}/M_1 \sim 0.5$, $[\text{O}/\text{Na}] \sim -0.15 - 0.42$, and for $M_{\text{gas}}/M_1 \sim 3.7$, $[\text{O}/\text{Na}] \sim 0.04 - 0.43$. Again, the $[\text{O}/\text{Na}]$ values do not match the full spread observed in GCs, but they are consistent with the observed second generation $[\text{O}/\text{Na}]$. A wind model that allows varying degrees of mixing between wind material and ambient gas is necessary to produce the full range of observed $[\text{O}/\text{Na}]$ values (Prantzos & Charbonnel 2006).

3 DISCUSSION

Throughout this paper, we have assumed a fiducial model for GCs and developed analytic criteria for the radiative cooling of mixed wind material and ambient gas to promote

formation of a second generation of stars. We have assumed a metallicity of one-tenth solar, no feedback processes other than energy and mass deposition of winds from massive, non-rotating stars, and only a single star formation event after the initial formation of the cluster. In this section, we examine how adjustments to our assumptions would impact our results.

3.1 Very Low Metallicities

The value of β_{crit} derived in equation (11) is dependent on the cooling function, which depends on the metallicity and relative metal abundances. Perhaps counter-intuitively, decreasing the metallicity of the first generation decreases β_{crit} because of changes in \dot{E}_w and \dot{M}_w , despite the decrease in the normalization of the cooling function. The fraction of the mixture that is made up of the wind material affects the overall gas metallicity, since massive star winds are enriched in certain H-burning byproducts, such as sodium and aluminum, and depleted in other elements such as oxygen and magnesium (Gratton et al. 2012). Indeed, we find that the metallicity of all metals in just the wind material in our fiducial cluster is about half that of solar, despite the first generation stars having one-tenth solar metallicity. This means that the critical mass-loading β_{crit} is actually dependent on the mass-loading itself. We have avoided this dependence in our analytic formulation by assuming a metallicity and checking that the mixture of wind material and ambient gas that we require has a metallicity somewhat similar to our assumption.

For example, using Sukhbold et al. (2016), winds from first-generation stars formed with one-tenth solar metallicity mixing with ambient gas of one-tenth solar metallicity, for our fiducial values of $M_{\text{gas}}/M_1 \sim 0.5-4$ when $\beta_{\text{wind}} = 1$, the mixture has a metallicity of ~ 0.11 solar due to the high metallicity of the wind. We assume this to be close enough to the value of $Z_{\text{gas}} = 0.1Z_{\odot}$ that we use for our analytic prescription. A more thorough analysis would involve tracking the wind metal species and adjusting the cooling function accordingly.

3.2 Other Feedback Processes

We have assumed that only the mass and energy of massive star winds contribute to the feedback processes in the GC. Theoretical and observational studies by, e.g., Murray et al. (2010); Lopez et al. (2011); Murray et al. (2011) show that radiation pressure on dust may blow gas out of GCs, and disrupt the host giant molecular cloud, on timescales less than a few Myr, before the first supernovae, potentially calling into question our assumption of a large reservoir of gas remaining for \sim Myr timescales after formation of the first stellar generation. However, the prevalence of dust in the mixture of gas in GCs likely depends on the metallicity of the gas; more dust forms at higher metallicities. Since radiation pressure is more effective at higher dust-to-gas ratios, higher metallicity clusters may inhibit second generation star formation by rapidly expelling gas. Strong radiation pressure feedback in high metallicity clusters may thus make low-metallicity GCs relatively more efficient at forming a second generation. An interesting avenue for further investigation would

be an analysis of all feedback processes in GCs and how they relate to secondary star formation in a time dependent model.

3.3 Asymptotic Giant Branch Stellar Winds

AGB winds have been examined as a potential source of material to form a second stellar generation (Ventura et al. 2001; Conroy & Spergel 2011; Conroy 2012) — like massive star winds, they are enriched in light element byproducts of hydrogen burning, and their low velocities allow the GC to retain them without requiring kinetic energy be lost to radiative cooling. Conroy et al. (2015) provide

$$\dot{M}_{\text{AGB}} \approx 10^{-4.1} M_{\odot} \text{ yr}^{-1} \left(\frac{M_1}{10^5 M_{\odot}} \right) \left(\frac{t_{\text{cl}}}{10^8 \text{ yr}} \right)^{-1.25} \quad (26)$$

$$\begin{aligned} \dot{E}_{\text{AGB}} &\approx 10^{33.9} \text{ erg s}^{-1} \\ &\times \left(\frac{M_1}{10^5 M_{\odot}} \right) \left(\frac{\sigma}{10 \text{ km s}^{-1}} \right)^2 \left(\frac{t_{\text{cl}}}{10^8 \text{ yr}} \right)^{-1.25} \end{aligned} \quad (27)$$

where t_{cl} is the age of the stellar cluster when AGB winds are active, σ is the velocity dispersion of the GC, and we have scaled \dot{M}_{AGB} and \dot{E}_{AGB} to our fiducial GC parameters and typical parameters for σ (McLaughlin & van der Marel 2005) and timescales for AGB winds. Substituting \dot{M}_{AGB} and \dot{E}_{AGB} into equation (11) gives $\beta_{\text{crit,AGB}} \sim 0.03$ and $\beta_{\text{crit,min,AGB}} \sim 0.01$ for $\alpha = 0.1$, and $\beta_{\text{crit,AGB}} \sim 0.15$ and $\beta_{\text{crit,min,AGB}} \sim 0.07$ for $\alpha = 1$. The critical condition on M_1/R_{cl} for AGB winds becomes $[M_1/R_{\text{cl}}]_{\text{crit,AGB}} \sim 10^3 \alpha_{0.1}^{2.7} \beta^{-3.7} M_{\odot} \text{ pc}^{-1}$. Since the necessary mass-loading for AGB winds to cool is very small, the winds will easily be able to cool without requiring additional mass-loading by ambient gas. However, the AGB winds scenario suffers from the same problems as the massive star winds scenario. In order to form a second generation with a half to three times as much mass as the first, assuming $\beta_{\text{wind}} = 1$,

$$\beta_{\text{AGB}} = \frac{M_2}{\dot{M}_{\text{AGB}}(R_{\text{cool}}/R_{\text{cl}})^3 \Delta t_{\text{AGB}}} \quad (28)$$

$$\begin{aligned} &\sim 20 \left(\frac{M_2}{2.5M_1} \right) \left(\frac{R_{\text{cool}}}{0.93R_{\text{cl}}} \right)^{-3} \left(\frac{\Delta t_{\text{AGB}}}{10^8 \text{ yr}} \right)^{-1} \\ &\times \left(\frac{\dot{M}_{\text{AGB}}}{10^{-4.1} M_{\odot} \text{ yr}^{-1}} \right)^{-1} \end{aligned} \quad (29)$$

where $\Delta t_{\text{AGB}} \sim 10^8 \text{ yr}$ is the length of time over which AGB winds are active, and we take $M_2 = 2.5M_1$ and $(R_{\text{cool}}/R_{\text{cl}})^3 = 0.8$. $\beta_{\text{AGB}} \sim 4-20$ corresponds to a mass of ambient gas of $M_{\text{gas}} \sim 0.5-5M_1$ (see equation 19), similar to the M_{gas} required by the massive star winds scenario when $\beta_{\text{wind}} = 1$. Unlike the massive star winds scenario, a high mass loading in the AGB winds scenario requires accretion of gas a hundred Myr after GC formation instead of mixing with leftover gas from the first generation of star formation (for a discussion of GC gas accretion scenarios, see e.g. Conroy & Spergel 2011). Both the massive star winds and the AGB winds scenarios may operate for a GC (D'Antona et al. 2016, find evidence for the AGB scenario in NGC 2808).

3.4 Rotating Star Wind Models

We examined the \dot{E}_w and \dot{M}_w used by STARBURST99 in the rotating models for one-tenth solar metallicity, in which stars rotate at 0.4 of break-up, originally presented in [Georgy et al. \(2013\)](#). \dot{M}_w and \dot{E}_w do not change significantly when stellar rotation is included, so the primary effect of including rotating star models is to increase the time until the first supernova that does not collapse directly to black hole by ~ 0.5 Myr, potentially prolonging the time over which second generation star formation can occur. However, in [Figure 7](#) we show that for much of the parameter space explored here, a second generation can form on a ~ 1 Myr timescale, so the additional ~ 0.5 Myr does not qualitatively change our results.

3.5 More Than Two Generations

Some GCs show evidence of more than two stellar populations (e.g., [Piotto et al. 2007](#); [Carretta et al. 2012](#); [Carretta 2015](#); [Milone et al. 2015](#)). Since we have found the second generation of stars may form in ~ 1 Myr after massive stars reach post-main sequence evolution, there is a possibility that more than two generations of stars may form in a single GC before supernovae pollute the gas in the GC with heavy elements $\sim 3 - 5$ Myr later. Since $\beta_{\text{crit}} \sim 1$, radiative cooling should again occur. However, a large β is again necessary for a substantial population to form. The wind material from massive second generation stars will be even more enriched with light element products of hydrogen burning than that from the first generation, or potentially AGB winds (see [§3.3](#)).

4 CONCLUSIONS

We have explored a model where winds from massive stars in globular clusters collide with each other and thermalize, then rapidly radiatively cool, forming a second generation of stars before the first supernovae (see also [Wünsch et al. 2008](#); [Palouš et al. 2014](#); [Wünsch et al. 2017](#)). We use the mass and energy deposition of massive stars and examine only winds that are produced before the first supernova that does not collapse to a black hole, because we find the second stellar generation can form well before supernovae are expected to occur. Our main results are:

- (i) The minimum mass-loading for any of the cluster's gas to cool and be retained within the cluster is given in [equation \(13\)](#). Thus, for $\beta \sim 1$, $\alpha \sim 0.1$, and $M_1/R_{cl} \gtrsim 10^5 M_\odot \text{pc}^{-1}$, no additional mass other than that provided by massive star winds is necessary for the winds to radiatively cool.
- (ii) The mass loading required for nearly all of the cluster to cool is just ~ 2 times higher than the minimum mass-loading for any of the cluster to cool ([equation 12](#)).
- (iii) For $\beta > \beta_{\text{crit}}$, the cluster wind's momentum and energy deposition rates (\dot{p}_w given by [equation 17](#) and \dot{E}_w given by [equation 16](#)) rapidly decrease as β increases. We speculate that a reduced cluster wind allows gas to remain within or in proximity to the cluster, and predict that low mass clusters should not have a second stellar generation ([Figure 8](#)).

- (iv) To produce a second stellar generation that is a half to three times larger than the first, a mass-loading of $\beta \sim 20 - 100$ is necessary, and does not strongly depend on M_1 , R_{cl} , or α . A high mass-loading can be provided by mixing the mass of wind material, which may be larger than expected from current stellar models in post-main sequence evolution, with an ambient gas mass leftover from the formation of the first stellar generation. $\beta \sim 20 - 100$ corresponds to $M_{\text{gas}}/M_1 \sim 0.5 - 4$ if wind mass loss rates are not enhanced. To produce a second generation mass fraction of $M_2/M_1 \sim 1$, a mass loading factor of $\beta \sim 30$, corresponding to $M_{\text{gas}}/M_1 \sim 1$ in our fiducial model, is needed. The onset time of supernovae, the mass ejection by winds, and the black hole formation probability for supernovae are uncertain. If all massive stars lose all of their pre-supernova mass as winds before the first supernovae, they drive a maximum mass-loss rate of $\dot{M}_{\text{max}} \sim 10^{-2.7} M_\odot \text{yr}^{-1}$. For \dot{M}_{max} , $\beta_{\text{crit}} \sim 0.8$ and the mass loading required to produce a second generation of size $M_2/M_1 \sim 0.5 - 3$ is $\beta \sim 7 - 40$, corresponding to $M_{\text{gas}}/M_1 \sim 0.5 - 3.7$.

- (v) The sum of the cooling and free-fall times for mass-loaded massive star winds are small, $\sim 1 - 2$ Myr, showing that the second generation can form before the first supernovae pollute the cluster gas with iron and other heavy elements.

- (vi) If winds mix with an amount of gas $M_{\text{gas}}/M_1 \sim 0.5 - 4$, the helium enhancement in the second generation is $\Delta Y \sim 0.002 - 0.013$, smaller than most observed helium spreads in globular clusters with multiple generations (see [Figure 10](#)). However, if high mass-loading is provided by enhancing massive star winds and mixing with ambient gas, the second generation helium enhancement is $\Delta Y \sim 0.004 - 0.023$ ([equation 24](#), dashed line in [Figure 10](#)) or $\Delta Y \sim 0.008 - 0.05$ for extreme assumptions about helium mass loss (dot-dashed line in [Figure 10](#)). He enhancement up to $\Delta Y \sim 0.16$ is possible if wind material does not mix with ambient gas at all, but this yields a smaller second generation fraction than observed values (see [Figure 10](#)). The values of $[\text{O}/\text{Na}] \sim -0.2 - 0.4$ for pure wind with no mixing and $[\text{O}/\text{Na}] \sim -0.1 - 0.16$ for mixing with maximal ambient gas mass $M_{\text{gas}}/M_1 \sim 4$ are consistent with the observed range of $[\text{O}/\text{Na}] \sim -1.5 - 0.5$ in second generations, but the range of $[\text{O}/\text{Na}]$ values produced is smaller in our model because we assume total mixing of wind material with ambient gas before any second generation stars are formed.

Rapid radiative cooling solves the problem of gas retention by GCs, and reduces the amount of extra mass needed by other self-enrichment scenarios to produce a large second generation, from $10 - 100$ times more mass ([Conroy 2012](#)) down to $0.5 - 4$ times more mass (although, only without fully reproducing observed second generation elemental abundances). Additionally, we do not require the extra mass needed to be in the form of first-generation stars, so our model does not require very large fractions (e.g. 96% in [Decressin et al. 2007b](#)) of first-generation stars to be preferentially ejected over second-generation stars, or very flat IMFs. The model predicts that ΔY is inversely proportional to the second generation mass fraction ([equation 24](#) and [Figure 10](#)) because mixing with ambient gas dilutes the enriched winds. Like other self-enrichment studies, our model cannot reproduce the abundance variations observed in GCs while simul-

taneously reproducing a massive second generation with a standard IMF, even under extreme assumptions about the total mass ejected by massive stars. A more complete understanding of the abundances and mass-loss rates of massive star winds may help to further reduce the problems of the many self-enrichment scenarios for second generation star formation.

ACKNOWLEDGMENTS

This work is supported in part by NSF grant 1516967. TAT thanks Dong Zhang for collaboration and discussion. CL thanks Jennifer A. Johnson, David H. Weinberg, and Laura A. Lopez for discussion of stellar feedback, and Tuguldur Sukhbold for discussion of wind abundances. We thank N. Bastian, E. Carretta, R. Wünsch, J. Palouš, G. Tenorio-Tagle, and S. Silich for constructive comments. We thank the anonymous referee for a timely and helpful report that improved the manuscript.

REFERENCES

- Bastian, N., Hollyhead, K., & Cabrera-Ziri, I. 2014, *MNRAS*, 445, 378
- Bastian, N., Cabrera-Ziri, I., & Salaris, M. 2015, *MNRAS*, 449, 3333
- Bastian, N. 2015, arXiv:1510.01330
- Bedin, L. R., Piotto, G., Anderson, J., et al. 2004, *ApJL*, 605, L125
- Boberg, O. M., Friel, E. D., & Vesperini, E. 2016, *ApJ*, 824, 5
- Bekki, K., & Mackey, A. D. 2009, *MNRAS*, 394, 124
- Caloi, V., & D’Antona, F. 2011, *MNRAS*, 417, 228
- Carretta, E., Bragaglia, A., Gratton, R. G., et al. 2009, *A&A*, 505, 117
- Carretta, E., Bragaglia, A., Gratton, R., D’Orazi, V., & Lucatello, S. 2009, *A&A*, 508, 695
- Carretta, E., Lucatello, S., Gratton, R. G., Bragaglia, A., & D’Orazi, V. 2011, *A&A*, 533, A69
- Carretta, E., Bragaglia, A., Gratton, R. G., Lucatello, S., & D’Orazi, V. 2012, *ApJL*, 750, L14
- Carretta, E., Bragaglia, A., Gratton, R. G., et al. 2014, *A&A*, 564, A60
- Carretta, E. 2015, *ApJ*, 810, 148
- Carretta, E. 2016, *The General Assembly of Galaxy Halos: Structure, Origin and Evolution*, 317, 97
- Chevalier, R. A., & Clegg, A. W. 1985, *Nature*, 317, 44
- Conroy, C., & Spergel, D. N. 2011, *ApJ*, 726, 36
- Conroy, C. 2012, *ApJ*, 758, 21
- Conroy, C., van Dokkum, P. G., & Kravtsov, A. 2015, *ApJ*, 803, 77
- D’Antona, F., Caloi, V., Montalbán, J., Ventura, P., & Gratton, R. 2002, *A&A*, 395, 69
- D’Antona, F., Bellazzini, M., Caloi, V., et al. 2005, *ApJ*, 631, 868
- D’Antona, F., Vesperini, E., D’Ercole, A., et al. 2016, *MNRAS*, 458, 2122
- Decressin, T., Meynet, G., Charbonnel, C., Prantzos, N., & Ekström, S. 2007, *A&A*, 464, 1029
- Decressin, T., Charbonnel, C., & Meynet, G. 2007, *A&A*, 475, 859
- de Mink, S. E., Pols, O. R., Langer, N., & Izzard, R. G. 2009, *A&A*, 507, L1
- Denisenkov, P. A., & Denisenkova, S. N. 1990, *Soviet Astronomy Letters*, 16, 275
- Denissenkov, P. A., & Hartwick, F. D. A. 2014, *MNRAS*, 437, L21
- D’Ercole, A., D’Antona, F., & Vesperini, E. 2011, *MNRAS*, 415, 1304
- Draine, B. T. 2011, *Physics of the Interstellar and Intergalactic Medium* by Bruce T. Draine. Princeton University Press, 2011. ISBN: 978-0-691-12214-4
- Ekström, S., Georgy, C., Eggenberger, P., et al. 2012, *A&A*, 537, A146
- Eldridge, J. J., Izzard, R. G., & Tout, C. A. 2008, *MNRAS*, 384, 1109
- Eldridge, J. J., & Stanway, E. R. 2009, *MNRAS*, 400, 1019
- Ferraro, F. R., Paltrinieri, B., Fusi Pecci, F., Rood, R. T., & Dorman, B. 1998, *ApJ*, 500, 311
- Georgy, C., Ekström, S., Eggenberger, P., et al. 2013, *A&A*, 558, A103
- Gratton, R. G. 1982, *A&A*, 115, 336
- Gratton, R. G., Bonifacio, P., Bragaglia, A., et al. 2001, *A&A*, 369, 87
- Gratton, R. G., Carretta, E., & Bragaglia, A. 2012, *A&A Rev.*, 20, 50
- Gratton, R. G., Lucatello, S., Sollima, A., et al. 2015, *A&A*, 573, A92
- Johnson, C. I., & Pilachowski, C. A. 2010, *ApJ*, 722, 1373
- Johnson, C. I., Rich, R. M., Pilachowski, C. A., et al. 2015, *AJ*, 150, 63
- Lamers, H. J. G. L. M., Snow, T. P., & Lindholm, D. M. 1995, *ApJ*, 455, 269
- Leitherer, C., Schaerer, D., Goldader, J. D., et al. 1999, *ApJS*, 123, 3
- Leitherer, C., Ekström, S., Meynet, G., et al. 2014, *ApJS*, 212, 14
- Lopez, L. A., Krumholz, M. R., Bolatto, A. D., Prochaska, J. X., & Ramirez-Ruiz, E. 2011, *ApJ*, 731, 91
- Loup, C., Forveille, T., Omont, A., & Paul, J. F. 1993, *A&AS*, 99, 291
- MacLean, B. T., Campbell, S. W., De Silva, G. M., et al. 2016, *MNRAS*, 460, L69
- Maeder, A., & Meynet, G. 2006, *A&A*, 448, L37
- Martell, S. L., Smolinski, J. P., Beers, T. C., & Grebel, E. K. 2011, *A&A*, 534, A136
- McLaughlin, D. E., & van der Marel, R. P. 2005, *ApJS*, 161, 304
- Milone, A. P. 2015, *MNRAS*, 446, 1672
- Milone, A. P., Marino, A. F., Piotto, G., et al. 2015, *ApJ*, 808, 51
- Milone, A. P., Piotto, G., Renzini, A., et al. 2017, *MNRAS*, 464, 3636
- Murray, N., Quataert, E., & Thompson, T. A. 2010, *ApJ*, 709, 191
- Murray, N., Ménard, B., & Thompson, T. A. 2011, *ApJ*, 735, 66
- Niederhofer, F., Bastian, N., Kozhurina-Platais, V., et al. 2016, arXiv:1609.01595
- Niederhofer, F., Bastian, N., Kozhurina-Platais, V., et al. 2016, arXiv:1612.00400
- Palouš, J., Wünsch, R., & Tenorio-Tagle, G. 2014, *ApJ*, 792, 105
- Pejcha, O., & Thompson, T. A. 2015, *ApJ*, 801, 90
- Piotto, G., Villanova, S., Bedin, L. R., et al. 2005, *ApJ*, 621, 777
- Piotto, G., Bedin, L. R., Anderson, J., et al. 2007, *ApJL*, 661, L53
- Prantzos, N., & Charbonnel, C. 2006, *A&A*, 458, 135
- Schaerer, D., & Charbonnel, C. 2011, *MNRAS*, 413, 2297
- Silich, S., Tenorio-Tagle, G., & Muñoz-Tuñón, C. 2003, *ApJ*, 590, 791
- Silich, S., Tenorio-Tagle, G., & Rodríguez-González, A. 2004, *ApJ*, 610, 226
- Sukhbold, T., Ertl, T., Woosley, S. E., Brown, J. M., & Janka, H.-T. 2016, *ApJ*, 821, 38
- Suntzeff, N. 1993, *The Globular Cluster-Galaxy Connection*, 48, 167

- Tenorio-Tagle, G., Silich, S., Rodríguez-González, A., & Muñoz-Tuñón, C. 2005, *ApJL*, 628, L13
- Tenorio-Tagle, G., Wünsch, R., Silich, S., & Palouš, J. 2007, *ApJ*, 658, 1196
- Valcarce, A. A. R., Catelan, M., Alonso-García, J., Cortés, C., & De Medeiros, J. R. 2014, *ApJ*, 782, 85
- van den Bergh, S. 1996, *ApJL*, 471, L31
- Ventura, P., D'Antona, F., Mazzitelli, I., & Gratton, R. 2001, *ApJL*, 550, L65
- Villanova, S., Piotto, G., King, I. R., et al. 2007, *ApJ*, 663, 296
- Wang, B. 1995, *ApJ*, 444, 590
- Woosley, S. E., & Weaver, T. A. 1995, *ApJS*, 101, 181
- Wünsch, R., Silich, S., Palouš, J., & Tenorio-Tagle, G. 2007, *A&A*, 471, 579
- Wünsch, R., Tenorio-Tagle, G., Palouš, J., & Silich, S. 2008, *ApJ*, 683, 683-692
- Wünsch, R., Palouš, J., Tenorio-Tagle, G., & Ehlerová, S. 2017, *ApJ*, 835, 60
- Zhang, D., Thompson, T. A., Murray, N., & Quataert, E. 2014, *ApJ*, 784, 93
- Zhang, C., Li, C., de Grijs, R., et al. 2015, *ApJ*, 815, 95